Quaternary Science Reviews 116 (2015) 57–71

Contents lists available at ScienceDirect

Quaternary Science Reviews

journal homepage: www.elsevier.com/locate/quascirev

Late Quaternary vegetation and climate dynamics at the northern limit of the East Asian summer monsoon and its regional and global-scale controls

Christian Leipe [a, **], Takeshi Nakagawa [b], Katsuya Gotanda [c], Stefanie Müller [a], Pavel E. Tarasov [a, *]

[a] Institute of Geological Sciences, Palaeontology, Freie Universität Berlin, Malteserstraße 74–100, Building D, 12249 Berlin, Germany
[b] Research Centre for Palaeoclimatology, Techno-complex Ritsumeikan University (BKC), 1-1-1 Noji-Higashi Kusatsu-shi, Shiga 525-8577, Japan
[c] Faculty of Policy Informatics, Chiba University of Commerce, 1-3-1 Ichikawa, Chiba 272-8512, Japan

ARTICLE INFO

Article history:
Received 23 August 2014
Received in revised form
14 March 2015
Accepted 16 March 2015
Available online

Keywords:
Quantitative climate reconstruction
Tree cover reconstruction
East Asian summer monsoon
Sakhalin Island
Holocene climate
Late Pleistocene climate

ABSTRACT

A late Quaternary pollen record from northern Sakhalin Island (51.34°N, 142.14°E, 15 m a.s.l.) spanning the last 43.7 ka was used to reconstruct regional climate dynamics and vegetation distribution by using the modern analogue technique (MAT). The long-term trends of the reconstructed mean annual temperature (TANN) and precipitation (PANN), and total tree cover are generally in line with key palaeoclimate records from the North Atlantic region and the Asian monsoon domain. TANN largely follows the fluctuations in solar summer insolation at 55°N. During Marine Isotope Stage (MIS) 3, TANN and PANN were on average 0.2 °C and 700 mm, respectively, thus very similar to late Holocene/modern conditions. Full glacial climate deterioration (TANN = −3.3 °C, PANN = 550 mm) was relatively weak as suggested by the MAT-inferred average climate parameters and tree cover densities. However, error ranges of the climate reconstructions during this interval are relatively large and the last glacial environments in northern Sakhalin could be much colder and drier than suggested by the weighted average values. An anti-phase relationship between mean temperature of the coldest (MTCO) and warmest (MTWA) month is documented during the last glacial period, i.e. MIS 2 and 3, suggesting more continental climate due to sea levels that were lower than present. Warmest and wettest climate conditions have prevailed since the end of the last glaciation with an optimum (TANN = 1.5 °C, PANN = 800 mm) in the middle Holocene interval (ca 8.7–5.2 cal. ka BP). This lags behind the solar insolation peak during the early Holocene. We propose that this is due to continuous Holocene sea level transgression and regional influence of the Tsushima Warm Current, which reached maximum intensity during the middle Holocene. Several short-term climate oscillations are suggested by our reconstruction results and correspond to Northern Hemisphere Heinrich and Dansgaard–Oeschger events, the Bølling–Allerød and the Younger Dryas. The most prominent fluctuation is registered during Heinrich 4 event, which is marked by noticeably colder and drier conditions and the spread of herbaceous taxa.

1. Introduction

The Asian monsoon, comprising the Indian and East Asian subsystem, is a major global atmospheric circulation system which principally controls the climate of a vast area stretching from the western Arabian Sea to the southern Russian Far East (RFE) including the most densely populated regions of the world (Alpat'ev et al., 1976; Wang, 2006). Palaeoclimate studies from both monsoon domains have outlined that climate conditions have varied significantly on different time-scales during the Holocene (e.g. Hu et al., 2008; Leipe et al., 2014) and last glacial period (e.g. Wang et al., 2001).

The spatiotemporal patterns and the magnitude of past variations in Asian monsoon activity and its relation with other components of the global climate system need further research (e.g. Nakagawa et al., 2008; Masson-Delmotte et al., 2013). To improve

* Corresponding author. Tel.: +49 30 838 70280; fax: +49 30 838 70745.
** Corresponding author. Tel.: +49 30 838 70271; fax: +49 30 838 70745.
E-mail addresses: c.leipe@fu-berlin.de (C. Leipe), ptarasov@zedat.fu-berlin.de (P.E. Tarasov).

http://dx.doi.org/10.1016/j.quascirev.2015.03.012
0277-3791/

our knowledge, additional climate reconstructions based on continuous long-term records from different regions of the Asian monsoon domain are required (e.g. Ju et al., 2007; Tarasov et al., 2011; Jin et al., 2014). To date, marine and terrestrial palaeoclimate proxy records from both the Indian summer monsoon (ISM) and East Asian summer monsoon (EASM) domains are mostly derived from the core monsoon zone and seldom exceed the Holocene interval (e.g. Morrill et al., 2003; Wang et al., 2005a; Herzschuh, 2006; Fleitmann et al., 2007; Wang et al., 2010; Ran and Feng, 2013 and references therein).

Especially from the northern EASM domain (ca 45–55°N), which covers parts of the northeast Asian continent and the north-western Pacific islands, the number of palaeoclimate studies is very scarce (e.g. Mokhova et al., 2009; Tarasov et al., 2011). In summer this area represents the transitional zone between cold air masses from high latitude polar regions and the warm and moist EASM air masses originating from the north-western Pacific. EASM influence here is strongest between June and July (Ding and Chan, 2005) when the monsoon front reaches its northernmost position at ca 55°N (Geograficheski Atlas SSSR, 1990). In winter, the climate is generally controlled by the East Asian winter monsoon (EAWM) (Alpat'ev et al., 1976). During this season, the region is situated on the boundary which separates the area to the south and to the north of ca 50°N where surface air temperature is significantly influenced by the Siberian High and the Arctic Oscillation, respectively (Wu and Wang, 2002).

Regional palaeoclimate studies available to the international community are based on a limited number of proxy records from sites in the southern RFE including the Amur river valley (e.g. Bazarova et al., 2008, 2011; Mokhova et al., 2009), Sakhalin (e.g. Igarashi et al., 2002; Takahara et al., 2010; Igarashi and Zharov, 2011), the Kuril Islands (e.g. Razjigaeva et al., 2013 and references therein) and the Japanese island of Hokkaido (e.g. Igarashi, 2013 and references therein). The majority of these works employed fossil pollen assemblages to provide qualitative interpretation of past climates and vegetation. Pollen records have also proved to be an excellent tool to quantify past variations in climate (e.g. Guiot, 1990; Jackson and Williams, 2004; Nakagawa et al., 2006) and vegetation cover (e.g. Prentice et al., 1996; Tarasov et al., 2000; Williams et al., 2011) in different parts of the world.

The so far longest terrestrial fossil pollen record Khoe, from the northernmost East Asian monsoon domain, has been obtained from a peat section on the north-western coast of Sakhalin (Fig. 1B) and spans the last ca 44 ka. Results of the conventional pollen and spore analysis are presented and discussed in a palaeoclimatological context by Igarashi et al. (2000, 2002). Later, this pollen record was also employed by Takahara et al. (2010) in their regional synthesis aimed to evaluate vegetation variability in response to Dansgaard–Oeschger (DO) events, and by Igarashi and Zharov (2011) to review the last glacial climate and vegetation dynamics on Hokkaido and Sakhalin. In this study we utilise the Khoe fossil pollen record for quantitative reconstruction of past climate conditions and tree cover using the modern analogue technique. The reconstruction results are compared with the published qualitative pollen-based vegetation and climate reconstructions and further discussed in the context of available regional and extra-regional palaeoclimate proxy records.

2. Environmental setting of Sakhalin

2.1. Location and climate conditions

Sakhalin is an island in the north-western Pacific (Fig. 1A). It is relatively narrow in shape but stretches ~950 km from north to south between ca 54.5° and 46°N. The island is separated from the continent by the ca 10 m deep Tatar Strait (~8 km at the narrowest point) in the northwest and from Hokkaido by the Soya Strait (~43 km at the narrowest point) in the south.

The climate of Sakhalin is mainly determined by a typical summer and winter monsoon circulation (Alpat'ev et al., 1976; Martyn, 1992). The summer monsoon is driven by low air pressure over Siberia (Asiatic Low) and high air pressure (Hawaiian High) over the northern Pacific Ocean. The development of both pressure systems results in the continuous northward migration of the East Asian polar front (Fig. 1A). This movement culminates in middle to late summer when the front stretches roughly from the northern tip of Sakhalin, over Mongolia, to eastern Kazakhstan. During this time, Sakhalin is affected by predominant flow of moist air masses from southern to south-eastern directions, which creates humid and thermally mild conditions (Fig. 1A). Due to the formation of the Aleutian Low and the Siberian High during autumn, the pressure gradient reverses and leads to the continuous southward migration of the East Asian polar front (Fig. 1A). In winter, when the pressure gradient is most pronounced, weather conditions on Sakhalin are predominated by south-eastward flow of continental cold and dry air masses. Simultaneously to the development of the Siberian High, the northern RFE is marked by enhanced cooling, which results in the southward shift of the Arctic front. In January it is approximately situated along the northern shore of the Okhotsk Sea (Alpat'ev et al., 1976; Geograficheski Atlas SSSR, 1990; Ivanov, 2002; Fig. 1A).

Another factor which affects the climate of Sakhalin involves the different thermal conditions of the surrounding seas driven by ocean currents (Fig. 1B). On the eastern coast of the island the East Sakhalin Cold Current (ESCC) flows southward. In the southwest and south of Sakhalin mean surface water temperatures are higher under the influence of the Tsushima Warm Current (TWC), which flows as a sub-branch of the Kuroshio Warm Current (KWC) northwards along the eastern margin of the Sea of Japan, and the Soya Warm Current (SWC), which flows as a TWC sub-branch between Sakhalin and Hokkaido towards the Okhotsk Sea. While the TWC gradually cools when progressing further north into the Tatar Strait, parts of the current turn and flow southwards along the shore of the Eurasian mainland as the Liman Cold Current (LCC).

Mean temperatures and precipitation generally follow a latitudinal gradient with highest values in the southern part of the island. The mean annual temperature (TANN) is 2.1 °C at Yuzhno-Sakhalinsk (46.97°N, 142.73°E, Fig. 1B) in the south, drops to 0.0 °C at Poronaysk (49.22°N, 143.10°E, Fig. 1B) and reaches only −2.4 °C at Okha (53.52°N, 142.91°E, Fig. 1B) in the north (Krestov, 2003). Mainly due to the maritime conditions and the influence of the TWC, winters are particularly mild in the narrow southern part of Sakhalin. The mean temperature of the coldest month (MTCO) in Yuzhno-Sakhalinsk is −13.8 °C, i.e. about six degrees higher than at Nogliki (51.81°N, 143.16°E, Fig. 1B) and Okha. A noticeable winter temperature gradient (and an increase in the continentality of climate) is also recognised between Sakhalin and the coastal areas of Asia. For example, the MTCO is −14.8 °C in Uglegorsk in western Sakhalin (49.08°N, 142.06°E, Fig. 1B), but only reaches −19.4 °C in Sovetskaya Gavan (48.97°N, 140.29°E, Fig. 1B) situated ~130 km westwards on the same latitude (Krestov, 2003). This feature should be considered during former intervals of low sea level when Sakhalin was not an island but a part of the Asian mainland. The global surface climate database (1961–1990 averages) of New et al. (2002) reveals that on Sakhalin ~60% of the mean annual precipitation (PANN) is received during the warm half of the year (April–September). While the PANN in Okha is ~550 mm, it is almost double (~960 mm) at Cape Krilion in the south (Krestov, 2003). Like the western coastal areas of Honshu and Hokkaido (Japan), the southern part of Sakhalin receives enhanced snow falls

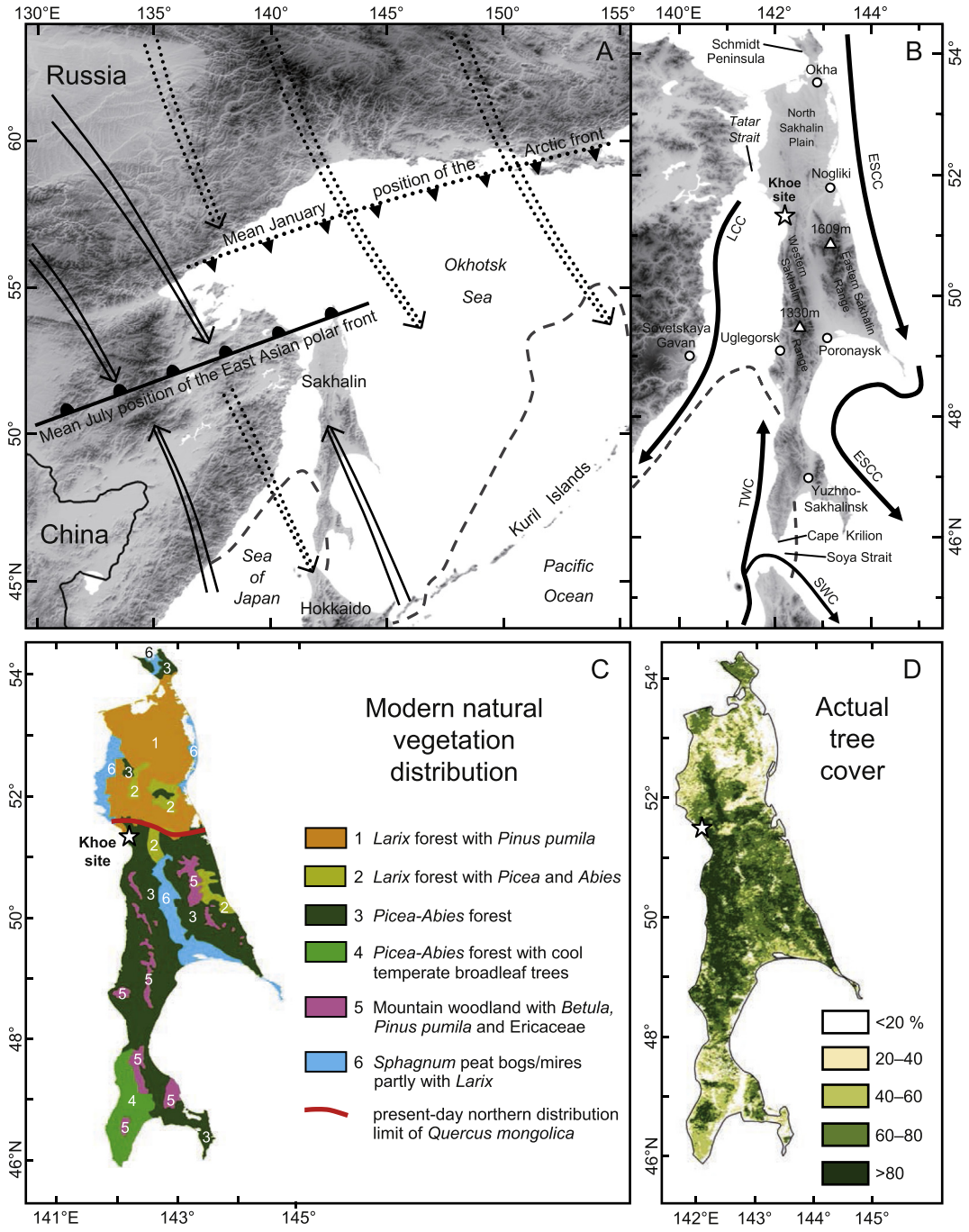

Fig. 1. (A) Overview map of the study region showing the mean July position of the East Asian polar front and the mean January position of the Arctic front together with the prevailing surface winds during summer (continuous arrows) and winter (dotted arrows) and (B) map of Sakhalin and adjacent regions illustrating the location of the Khoe sedimentary succession marked by a star; geographic features mentioned in the text; and schematic ocean currents including the East Sakhalin Cold Current (ESCC), the Liman Cold Current (LCC), the Tsushima Warm Current (TWC) and the Soya Warm Current (SWC) (according to Boyd, 1995). The boundary of the mean maximum extent of sea ice cover in the Okhotsk Sea and the Tatar Strait is indicated in both maps by a broken line (according to Geograficheski Atlas SSSR, 1990). (C) Actual vegetation map of Sakhalin (simplified after Bukhteeva and Reimers, 1967). (D) The AVHRR-derived total woody coverage of Sakhalin (after DeFries et al., 2000a, 2000b).

promoted by the predominance of winter monsoon winds which transport significant amounts of moisture absorbed over the relatively warm Sea of Japan.

2.2. Vegetation

The cool and humid climate promoted the growth of boreal and temperate forests, which cover most of the island. North of ca 51.5°N, Sakhalin is dominated by *Larix gmelinii* (Dahurian larch) cold deciduous forest and evergreen shrubs of *Pinus pumila* (Siberian dwarf pine) (Fig. 1C). The area to the south is mainly covered by dense evergreen forests (i.e. taiga) with *Picea jezoensis* (Jezo spruce) and *Abies sachalinensis* (Sakhalin fir) as the main components. As far as ca 48°N these conifer forests are dominated by *P. jezoensis* and further south by *A. sachalinensis*. An exception is the northernmost part of Sakhalin (i.e. the Schmidt Peninsula, Fig. 1B), where *P.*

jezoensis forms stands with *L. gmelinii* and *P. pumila*. The south-westernmost end of Sakhalin is characterised by mixed forests comprising evergreen conifers (mostly *A. sachalinensis*) and temperate deciduous broadleaf trees like *Acer mono* (Painted maple), *Fraxinus mandshurica* (Manchurian ash), *Juglans ailantifolia* (Japanese walnut), *Juglans mandshurica* (Manchurian walnut), *Kalopanax septemlobus* (Prickly castor oil tree), *Phellodendron sachalinense* (Sakhalin corktree), *Quercus mongolica* (Mongolian oak), *Quercus crispula* (Japanese oak), *Tilia japonica* (Japanese lime) and *Ulmus japonica* (Japanese elm) (Bukhteeva and Reimers, 1967; Alexandrova, 1982; Krestov, 2003; Nakamura and Krestov, 2005). However, *Q. mongolica*, *Ulmus laciniata* (Manchurian elm) and *U. japonica* may grow sporadically in climatically favourable locations within the taiga forest zone, as far north as ca 51.5°N (Sokolov et al., 1977). Higher elevations south of ca 51.5°N are characterised by mountain woodland with open *Betula ermanii* (Erman's birch) forest and shrubland with *P. pumila* and shrubby Ericaceae like *Empetrum nigrum* (crowberry) and *Rhododendron* spp. (azalea). Wetlands are a common feature of the coastal and fluvial landscapes of Sakhalin. The most widespread are *Sphagnum* (peat moss) peat bogs of up to 7 m thickness with *Larix*, *Salix* (willow), *Alnus* (alder) and *Myrica* (bayberry) growing on the ridges (Bukhteeva and Reimers, 1967; Zhulidov et al., 1997).

3. Data and methods

3.1. Study site and fossil pollen record

The pollen record presented in this study was obtained from a coastal cliff, which is located ~3 km north of the settlement of Khoe (51.34°N, 142.14°E, 15 m a.s.l.) on the western coast of Sakhalin facing the Tatar Strait (Fig. 1B). There is no permanent climate station in the vicinity of Khoe. The modern climate conditions derived from the New et al. (2002) dataset for the 10′ × 10′ grid surrounding the sampling site are characterised by MTCO, MTWA, TANN and PANN values of −18.5 °C, 16.4 °C, 0.2 °C and 625 mm, respectively. Altogether, 113 samples were collected from a sedimentary succession situated in a tectonic depression in the Khoe area (see Igarashi et al., 2000, 2002; Igarashi and Zharov, 2011 for further details). The succession primarily consists of peat, clay, silt and sandy layers (Fig. 2; Igarashi et al., 2000, 2002).

A total of 42 arboreal (AP) and non-arboreal (NAP) terrestrial pollen types, three aquatic taxa and spores from six types of ferns and fern allies were identified. In the simplified pollen diagram (Fig. 2) percentages of individual pollen taxa are calculated upon the total sum of all terrestrial AP and NAP taxa, and percentages of individual spore types are calculated using the total sum of terrestrial pollen and spores. For plotting both fossil and modern pollen percentage diagrams, we employed the Tilia/Tilia-Graph/TGView software package (Grimm, 1993, 2004).

3.2. Radiocarbon dates and core chronology

Eight radiocarbon dates were obtained from the sedimentary succession from Khoe (Table 1). For the present study, we converted ^{14}C ages into calendar (cal.) ages (Table 1) using the online version of the CalPal radiocarbon calibration program (Danzeglocke et al., 2013) and the software-based CalPal-2007 program (Weninger and Jöris, 2008; Weninger et al., 2013). The radiocarbon dates suggest that the Khoe sedimentary succession represents the last ca 43.7 ka. For the Holocene part there are five ^{14}C dates (Table 1) available. Taking into account the overall pattern of these dates in relation to depth, the ^{14}C age of the sample at 302.5 cm depth (9420 ± 50 ^{14}C yr BP) appears to be displaced towards older ages, which may be the result of contamination. We consequently excluded it from the age–depth model (Fig. 2). The chronology for the Holocene part was defined by linear interpolation based on the calibrated ages of the remaining four ^{14}C dates.

The Marine Isotope Stage (MIS) 2 and 3 interval in the Khoe record is represented by three radiocarbon dates (Table 1). Previous studies have shown that late Pleistocene–Holocene temperature records from the North Atlantic region are consistent with reconstructions from the Asian monsoon domain (e.g. Porter and An, 1995; Wang et al., 2001; Zhao et al., 2003; Dykoski et al., 2005; Nakagawa et al., 2005). Pronounced climate fluctuations (i.e. DO and Heinrich events) reported from the North Atlantic region were also identified by variations in the relative abundances of AP types in the fossil pollen records from the north-western Pacific by Takahara et al. (2010). This encouraged us to use the well-dated mean annual temperature reconstruction from central Greenland (Alley, 2000) and the TANN curve derived from the Khoe pollen record (this study) to further confine the chronology for the pre-Holocene part of the sedimentary succession by means of stadial and interstadial temperature oscillations. Though, we have done our best to put forward as strong an age model as possible given the limitations of available radiometric dates and problems of using a peat, a potentially high level of chronological uncertainty remains for the glacial part of the Khoe record. However, given the importance of this region in understanding the East Asian summer monsoon and the apparent antiquity and high quality of the Khoe pollen record, our pollen-based reconstructions and interpretations can be offered as a framework for further testing.

3.3. Modern pollen data

We employed a set of modern pollen spectra from existing reference datasets from Eurasia (Tarasov et al., 1998, 2005) and the southern (Mokhova et al., 2009) and northern (Edwards et al., 2000) RFE that have been used in previous studies for quantitative vegetation and climate reconstructions (e.g. Bigelow et al., 2003; Andreev et al., 2004; Tarasov et al., 2011; Williams et al., 2011; Melles et al., 2012). The sites of the pollen samples are distributed over four major regions of the RFE including the south-eastern Sakha Republic, the southern Magadan Oblast, the southern Khabarovsk Krai and Sakhalin covering a broad range of vegetation and climate conditions. Calculation of relative pollen abundances for each spectrum was based upon the total sum of terrestrial pollen.

3.4. Pollen-based climate and tree cover reconstruction

Based on the modern analogue technique (MAT, Overpeck et al., 1985; Guiot, 1990), we reconstruct four main climate variables (MTCO, MTWA, TANN and PANN) and percentage total tree cover. Performance tests (cross-validation) revealed a reasonably high correlation between pollen-inferred and observed climate variables for modern reference datasets from Japan and the southern RFE (R^2 = 0.79–0.91; Tarasov et al., 2011), eastern Siberia and the northern RFE (R^2 = 0.72–0.81; Melles et al., 2012). Similarly strong correlations are obtained for percentage total tree cover using modern pollen datasets from north-eastern Eurasia (R^2 = 0.77; Tarasov et al., 2007) and China (R = 0.83; Zheng et al., 2010). This suggests the high potential for reliable reconstruction of these environmental parameters from fossil pollen assemblages. The climate variables were attributed to the reference pollen sampling sites by interpolation (Inverse Distance Weighting) from the global high-resolution (10′ × 10′ grid size) dataset of surface climate averaged over a thirty-year (1961–1990) period from New et al. (2002) using free-access Polation software (Nakagawa et al., 2002; http://dendro.naruto-u.ac.jp/). For estimating the thermal

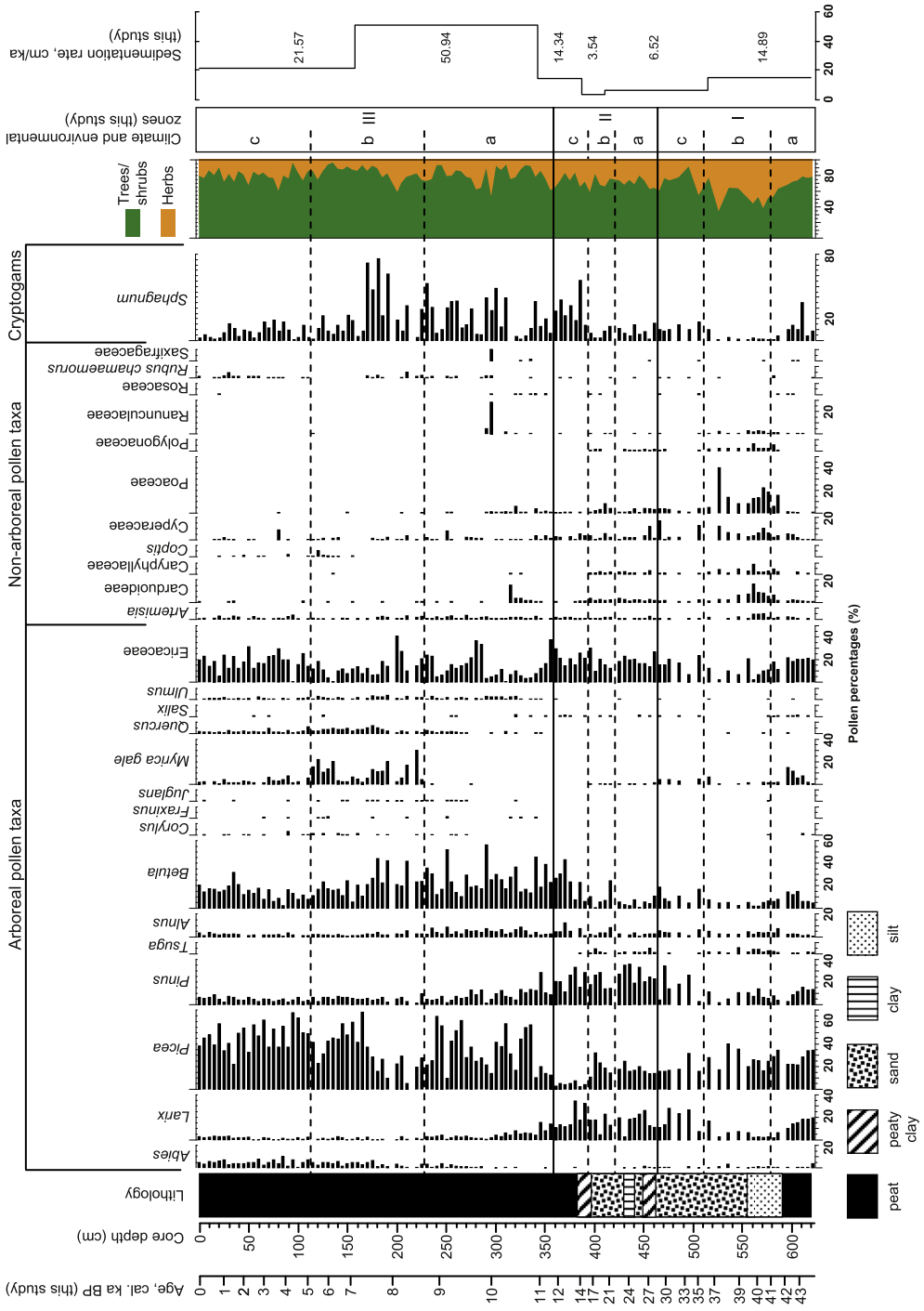

Fig. 2. Simplified percentage pollen and spore diagram representing the 113 fossil pollen spectra from the Khoe sedimentary succession (redrawn using the data of Igarashi and Zharov, 2011) along with the simplified lithology (according to Igarashi et al., 2002). The age axis (cal. ka BP) and average sedimentation rates (cm/ka) reflect the age-depth model used in the current study. Units Ia–IIIc illustrate climate and environmental zonation as revealed by the MAT reconstructions (Fig. 4) and discussed in the text.

variables, we accounted for a standard temperature lapse rate of −0.6 °C per 100 m difference in altitude (Domrös and Peng, 1988).

To reconstruct past changes in total tree cover, we utilised the satellite-based Advanced Very High Resolution Radiometer (AVHRR) dataset with a spatial resolution of 0.5′ × 0.5′ providing the estimated percent area covered by woody vegetation, herbs and bare ground (DeFries et al., 2000a, 2000b). Surface coverage values in the dataset range between 0 and 80% with the value of 80% corresponding to a coverage of ≥80% (Fig. 1D). Williams and Jackson (2003) have demonstrated that results of pollen-based reconstructions correspond best to satellite-based estimates of woody cover within a window size ranging from 20 × 20 to 150 × 150 km. Later, Tarasov et al. (2007) obtained highest correlations for northern Eurasia using a search window of 21 × 21 km (~441 km^2), which was recently confirmed for China by Zheng et al. (2010). Therefore, we first defined a “geodesic” (equal area) buffer with a radius of 11.85 km (~441 km^2) around each reference pollen

Table 1
Radiocarbon dates for samples from the Khoe sediment profile (Igarashi et al., 2002; Igarashi and Zharov, 2011) and calibrated ages assigned to samples of the Khoe profile based on the correlation between annual temperature reconstructions from Khoe (this study) and central Greenland (Alley, 2000). Calibrations were performed using CALPAL-2007 (Weninger and Jöris, 2008; Weninger et al., 2013) and the online version of the CalPal radiocarbon calibration program (Danzeglocke et al., 2013). Ages marked by an asterisk were used in the age–depth model applied in this study.

Laboratory ID	Composite depth (cm, mid point)	Dated material	Radiocarbon date, ^{14}C BP	Calibrated age, cal. BP	Reference	CalPal age, cal. BP	Error range (95% conf. interval)	
							Upper age limit, cal. BP	Lower age limit, cal. BP
IAAA 62612	157.5	Plant fragment	6330 ± 40	7262	Igarashi and Zharov, 2011	7255*	7160	7360
KIA 9557	252.5	Plant fragment	8251 ± 62	9229	Igarashi et al., 2002	9246*	9020	9460
IAAA 72344	302.5	Plant fragment	9420 ± 50	10,651	Igarashi and Zharov, 2011	10,653	10,520	10,800
IAAA 72345	342.5	Bulk TOC	9520 ± 50	10,854	Igarashi and Zharov, 2011	10,887*	10,580	11,180
IAAA 72346	357.5	Plant fragment	10,020 ± 50	11,514	Igarashi and Zharov, 2011	11,535*	11,250	11,810
KIA 9558	387.5	Plant fragment	12,000 ± 101	13,865	Igarashi et al., 2002	13,989*	13,610	14,330
–	395.0	–	–	15,950*	Alley, 2000	–	–	–
–	405.0	–	–	19,250*	Alley, 2000	–	–	–
–	410.0	–	–	20,300*	Alley, 2000	–	–	–
–	430.0	–	–	23,400*	Alley, 2000	–	–	–
KIA 9559	432.5	Organic mud	20,050 ± 230	24,009	Igarashi et al., 2002	23,974*	23,400	24,600
–	435.0	–	–	24,100*	Alley, 2000	–	–	–
–	445.0	–	–	25,600*	Alley, 2000	–	–	–
–	465.0	–	–	29,000*	Alley, 2000	–	–	–
–	470.0	–	–	29,700*	Alley, 2000	–	–	–
–	475.0	–	–	30,500*	Alley, 2000	–	–	–
–	495.0	–	–	33,600*	Alley, 2000	–	–	–
–	515.0	–	–	36,400*	Alley, 2000	–	–	–
–	535.0	–	–	38,300*	Alley, 2000	–	–	–
–	560.0	–	–	39,700*	Alley, 2000	–	–	–
–	580.0	–	–	41,130*	Alley, 2000	–	–	–
–	585.0	–	–	41,600*	Alley, 2000	–	–	–
Beta 122027	607.5	Organic debris	37,270 ± 750	42,365	Igarashi et al., 2002	42,007	41,090	42,970*

sampling site using the ArcGIS v10.0 software package (ESRI, 2012). In a second step, the AVHRR total tree cover estimates of all grid cells situated within each buffer were arithmetically averaged and assigned to the appropriate reference pollen spectrum.

Each terrestrial pollen taxon in the Khoe fossil pollen record (Igarashi et al., 2000) appears in the employed pollen reference dataset. Thus, all taxa were considered in the MAT application. Prior to method application, all pollen abundances were square root transformed in order to further enhance minor taxa. The similarity between each assemblage of the Khoe fossil pollen record and each of the spectra in the modern reference dataset was numerically measured by squared chord distance (SCD) (Overpeck et al., 1985; Guiot, 1990). As was frequently done in applications of the existing modern pollen reference dataset (Nakagawa et al., 2002; Tarasov et al., 2007, 2011; Melles et al., 2012), we considered a number of eight best modern analogues. A weighted average was applied to the climate values and percentage tree cover of the modern analogues. The range of the variables associated with the eight best modern analogues is regarded as the uncertainty (i.e. error) interval. Calculation of the dissimilarities was performed with the aid of the computer program C2 v1.6.8 (Juggins, 2007).

4. Results and interpretation

All eight best modern analogues assigned to the fossil pollen samples are allocated within the area between 46.34 and 62.70°N and 130.00–152.33°E, which roughly corresponds to the spatial window shown in Fig. 1A. The modern reference data set from this area comprises of 236 surface samples (Fig. 3). MAT-based annual and seasonal temperature reconstructions reveal that TANN is basically controlled by MTCO. Temperature (MTCO and MTWA), precipitation (PANN) and tree cover reconstruction results from the Khoe site (Fig. 4A, B, D, E) are briefly summarised below with regard to the fossil pollen assemblages (Fig. 2). The boundaries of the identified zones (roughly corresponding to the MIS boundaries) and subzones (Ia–IIIc) defined on the basis of the climate and environmental reconstruction results are plotted in Fig. 2. For information on the visually defined pollen zones, the reader is referred to Igarashi et al. (2002) and Igarashi and Zharov (2011).

The interval ca 43.7–41.9 cal. ka BP (620–590 cm, unit Ia) is marked by relatively high average values for PANN ranging between 675 and 705 mm and average values for MTCO ranging between −18.5 and −17.4 °C. The error ranges are relatively small. Reconstructed total tree cover is lower than present and ranges between 44 and 52%, suggesting a forested landscape. The pollen assemblage shows a predominance of *Picea* accompanied with *Pinus*, *Larix* and *Betula*, and very low percentages of *Abies* and *Tsuga* (Igarashi et al., 2002), indicating boreal conifer forests with larch and spruce growing around the study site (Igarashi and Zharov, 2011). Relatively high percentages of *Sphagnum* moss spores and peat accumulation (Fig. 2) suggest moist environments, in line with the quantitatively reconstructed PANN values and qualitative interpretation of the local climate as maritime (Igarashi and Zharov, 2011).

At ca 41.9–38.6 cal. ka BP (590–540 cm, unit Ib), the reconstruction indicates very cold and dry climate, with PANN and MTCO values of 410 mm and −36 °C, respectively. By contrast, MTWA values are relatively high (18 °C), pointing to more continental than present conditions around the Khoe site. With minimum values of approximately 30%, total tree cover reconstruction suggests a more open than present (though still forested) landscape. The pollen assemblage of this interval also demonstrates highest percentages for herbaceous taxa and drop in AP taxa percentages (Fig. 2), suggesting strengthening of cold grassland communities (Igarashi and Zharov, 2011). In agreement with these interpretations, *Sphagnum* percentages dropped significantly (Fig. 2) and peat accumulation was interrupted by accumulation of predominantly inorganic silty and sandy material (Igarashi and Zharov, 2011), likely indicating colder and drier environments.

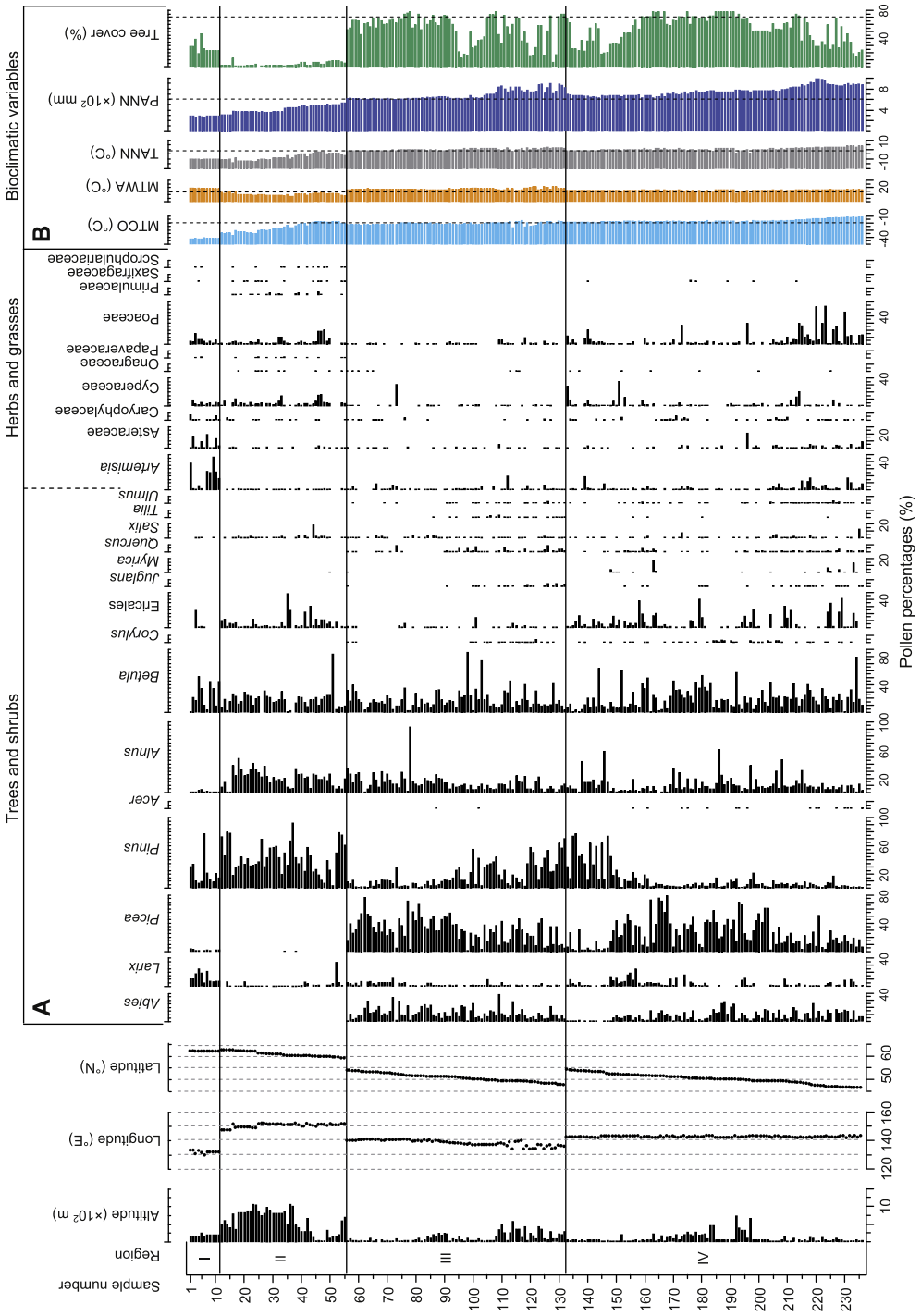

Fig. 3. Summary chart showing (A) the simplified percentage pollen diagram including 236 continuously numbered modern pollen spectra from the study area grouped by sample source area (I – Sakha Republic, II – Magadan Oblast, III – southern Khabarovsk Krai, IV – Sakhalin) and sorted within each group by latitudinal position (north to south). (B) Main climate variables and percentage modern tree cover are inferred from the New et al. (2002) modern climate dataset and the AVHRR-derived dataset from DeFries et al. (2000a, 2000b). MTCO = mean temperature of coldest month, MTWA = mean temperature of warmest month, TANN = mean annual temperature and PANN = mean annual precipitation.

The subsequent interval between ca 38.6 and 29 cal. ka BP (540–467.5 cm, unit Ic), demonstrates a return to moderately high temperature and precipitation values similar to the values reconstructed for the bottommost unit Ia (620–590 cm). This is paralleled by relatively high but slightly decreasing tree cover percentages. The pollen assemblage also reveals increased, though fluctuating, percentages of *Larix* and *Pinus* and relative decrease in *Picea* and Cyperaceae pollen percentages.

During ca 29 and 22 cal. ka BP (467.5–420 cm, unit IIa) the thermal and precipitation reconstructions show considerably more fluctuations and larger uncertainty intervals. This suggests at least several excursions towards generally colder and drier conditions. Tree cover reconstruction shows higher variability and a noticeable decrease after ca 28 cal. ka BP. While *Larix* and *Picea* percentages are comparable to unit Ic, *Pinus* relatively increases.

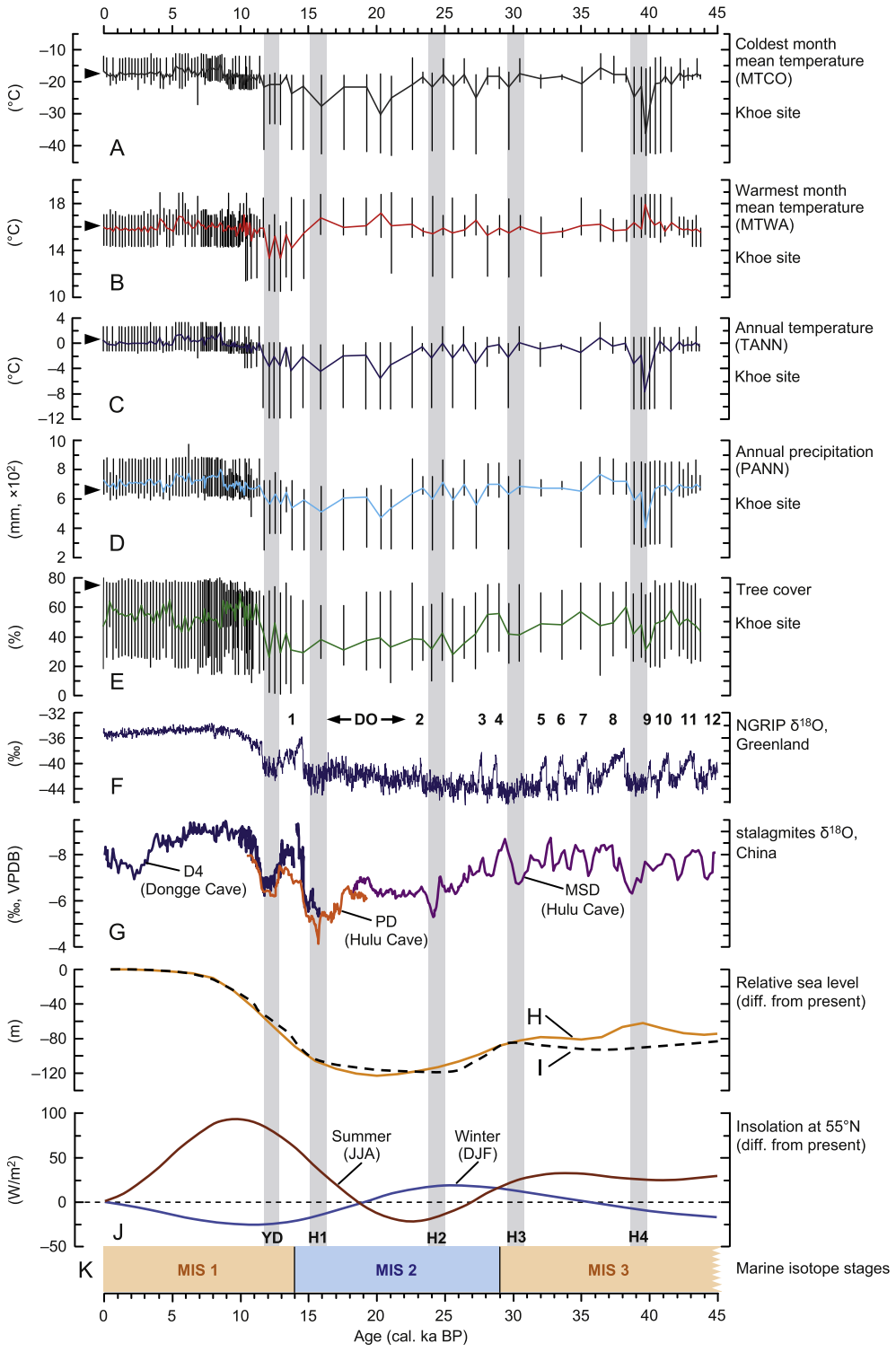

Fig. 4. Results of the pollen-based climate and tree cover reconstructions from Khoe, Sakhalin (A–E, this study) with curves indicating weighted mean averages of reconstructed variables and vertical lines representing error bars or the analogue uncertainty range defined by the minimum and maximum value of the eight best modern analogues assigned to each analysed fossil sample. Other climate records include (F) the NGRIP ice core (75.10°N, 42.32°W, 2917 m a.s.l.) $\delta^{18}O$ record (according to Svensson et al., 2008) with Dansgaard–Oeschger (DO) events (according to Dansgaard et al., 1993); (G) the stalagmite $\delta^{18}O$ records PD and MSD from Hulu cave (23.50°N, 119.17°E, 100 m a.s.l., according to Wang et al., 2001) and D4 from Dongge cave (25.28°N, 108.08°E, 680 m a.s.l., according to Yuan et al., 2004) in China; (H) the reconstructed (Waelbroeck et al., 2002) and (I) ICE-5G(VM2) model simulated (Peltier and Fairbanks, 2006) changes in relative global sea level. (J) shows the computed mean summer (June–August) and winter (December–February) insolation at 55°N (according to Laskar et al., 2004). (K) Marine Isotope Stages (MIS) are illustrated according to Lisiecki and Raymo (2005). Heinrich events H1 to H4 (according to Heinrich, 1988) and the Younger Dryas (YD) are indicated by grey bars.

The reconstruction results indicate a phase of significant climate deterioration between ca 22 and 15.3 cal. ka BP (420–392.5 cm, unit IIb) with lower MTCO (down to −30 °C) and PANN values (down to 470 mm). Reconstructed tree cover persists on relatively low levels of 35%, though boreal woody plants still play a significant role in the vegetation cover, despite increased landscape openness. In line with the reduced precipitation and colder winter conditions, the percentages of *Larix* and *Picea* during this phase are relatively high and low, respectively. Although *Larix* reached maximum and *Picea* minimum values of the whole record between the interval ca 15.3 and 12.8 cal. ka BP (392.5–372.5 cm, lower unit IIc), mean values of the climate reconstruction suggests most unfavourable conditions around 20 cal. ka BP. The trend of climate amelioration suggested by the increase in PANN (up to 640 mm) and TANN (up to −1 °C) parallelled by a decrease in seasonality (MTCO up to −18.5 °C, MTWA down to 13.5 °C) is interrupted by a climate reversal with slightly colder climate conditions between ca 12.8 and 11.7 cal. ka BP (372.5–357.5 cm, upper unit IIc).

The interval between ca 11.7 and 8.7 cal. ka BP (357.5–227.5 cm, unit IIIa) shows continuous peat accumulation in the sediment column and progressively improving climate conditions, which are wetter and warmer compared to the lower part of the Khoe section, i.e. MTCO (−21 to −17 °C), MTWA (14.5–17 °C) and PANN (620–720 mm). The average tree cover density of ca 60% reflects spread of forests in the area. Simultaneously, pollen assemblages show abrupt increase in *Betula* and *Picea* and decrease in *Larix* and *Pinus*, indicating a shift to warmer/wetter conditions. The warming trend is also confirmed by pollen of thermophilous broadleaf woody taxa (i.e. *Quercus* and *Ulmus*), which start to appear in the lower part of this interval. Cool temperate taxa and temperate taxa become more diverse and abundant (Fig. 2) above 322.5 cm (ca 10.5 cal. ka BP), though *Picea* and *Betula* remain dominant taxa.

Most favourable climate conditions are reconstructed between ca 8.7 and 5.2 cal. ka BP (227.5–112.5 cm, unit IIIb). Compared to the previous part of the record, average MTCO, MTWA and PANN are higher by about 2.5 °C, 0.5 °C and 70 mm, respectively. Average total tree cover around 50% is slightly lower than in the previous interval, which might reflect a more open nature of the cool mixed forest in comparison to the dense boreal conifer forest. Pollen assemblages reveal highest percentages of *Quercus* and *Ulmus* pollen within this interval (Fig. 2). Pollen of *Myrica gale* (bog myrtle) – a deciduous shrub typically growing in acidic peat bogs – show highest percentages within the whole record, likely pointing to an open shrubland and mire environments at and around the site.

In the topmost part of the record (ca 5.2 cal. ka BP to present; 112.5–0 cm, unit IIIc), the reconstructed climate variables show a slight deterioration of the climate conditions and slightly higher tree cover than in the previous unit. The pollen assemblage of this interval (Fig. 2) shows a dominance of *Picea* and *Abies* and high values of Ericaceae pollen, whereas percentages of temperate woody taxa and *M. gale* decrease.

5. Discussion

5.1. Late Quaternary vegetation and climate dynamics in northern Sakhalin

The refined Khoe chronology illustrates a shift to significantly higher sedimentation rates (Fig. 2) and onset of peat accumulation at the boundary between MIS 2 and 1 (i.e. around 14 cal. ka BP; Lisiecki and Raymo, 2005, Fig. 4K) and a further increase in sedimentation rate at the Lateglacial–Holocene transition (i.e. around 11.7 cal. ka BP). Another noticeable change from silty to sandy sediment occurs about 27.5 cal. ka BP, shortly after the transition from the MIS 3 interstadial to the MIS 2 full glacial interval dated to ca 29 cal. ka BP in the marine isotope records (Lisiecki and Raymo, 2005, Fig. 4K), supporting the temperature-tuned Khoe chronology during the late Pleistocene interval.

For chronological comparison, the results of the quantitative climate and tree cover reconstructions together with selected palaeoclimate records and insolation parameters are plotted along their original age axis in Fig. 4. On a broader time scale, the reconstruction results allow a rough subdivision of the Khoe vegetation and climate records into two milder and moister intervals, i.e. ca 43.7–29 cal. ka BP (620–467.5 cm, unit I in Fig. 2) and ca 11.7–0 cal. ka BP (357.5–0 cm, unit III in Fig. 2) interrupted by noticeably colder and drier period (unit II in Fig. 2), which broadly correspond to the later part of the MIS 3 interstadial, the Holocene interglacial and the full glacial interval, respectively.

The MAT-based climate reconstruction at Khoe shows that during the late Pleistocene, TANN mainly reflects changes in winter temperatures, which are represented by MTCO. This corresponds with climate reconstructions from other regions of the Northern Hemisphere (NH) including North America and Northern Eurasia (e.g. Tarasov et al., 1999; Bartlein et al., 2011; Helmens, 2014). In our reconstructions, PANN is parallelled by MTCO. This matches the long-term relationship between the reconstructed TANN and PANN variation over the last ca 450 ka in central Japan, which was determined by Nakagawa et al. (2008). The Khoe pollen-based climate reconstruction also demonstrates relatively high average MTWA values during the MIS 2 and MIS 3 intervals. Though, relatively warm glacial summers were reconstructed by different proxies in other regions of northern Asia (e.g. Kageyama et al., 2001; Kienast et al., 2005; Müller et al., 2014) in line with more continental climate conditions, the degree of warmth should not be overestimated since the error ranges, especially during MIS 2, leave a potential for colder than present summer temperatures. It has to be noted that the generally larger error ranges during the late Pleistocene, and especially during MIS 2, might be the result of weaker modern analogues or/and a greater range of bioclimatic tolerance of the past and present vegetation communities representing cold and dry regions of Asia (e.g. Prentice et al., 1992; Müller et al., 2014).

The cold winters and relatively warm summers suggested by the MTCO and MTWA reconstructions during the late Pleistocene are supported by an analysis of the full set of the Paleoclimate Modelling Intercomparison Project (PMIP) simulations for the Last Glacial Maximum (LGM) (Jiang and Lang, 2010). For the Sakhalin region, the averaged simulation results demonstrate much stronger temperature anomalies during winter (ca −10 to −15 °C) than during summer (ca −4 to −3 °C). These anomalies are well within the reconstructed temperature ranges (Fig. 4A, B).

The derived climate and tree cover reconstructions for the Holocene interval are marked by comparably small error ranges. The relationship between MTCO and MTWA follows a different pattern. Unlike the late Pleistocene period, variations in both parameters appear to be in phase. This is probably a result of rising sea level, which led to a reduction in continentality.

The following sections provide a more detailed discussion on the pollen-inferred changes in vegetation and climate in view of the previously published regional and extra-regional palaeoclimate and palaeoenvironmental proxy records in chronostratigraphical order. Given the relatively coarse resolution of the Khoe record, emphasis is put on long-term trends and on multicentury-scale climate oscillations.

5.2. The MIS 3 interstadial (ca 43.7–29 cal. ka BP)

Despite the very cold and dry conditions suggested around H4 (ca 41.9–38.6 cal. ka BP), the long-term average temperature and

precipitation reconstructions with relatively small error ranges attest the MIS 3 interval of the Khoe record as representing relatively moist and thermally mild climate conditions (Fig. 4A–D) favourable for tree growth (Fig. 4E). Compared to Holocene conditions, NAP taxa played a more important role in the regional vegetation (Fig. 2; Igarashi and Zharov, 2011). The weighted averages of the pollen-derived climate variables during the MIS 3 interstadial are close to modern ones. The Hulu Cave MIS 3 $\delta^{18}O$ values (Wang et al., 2001, MSD in Fig. 4G) are more or less identical with the modern and slightly higher than the early to middle Holocene optimum $\delta^{18}O$ values from Dongge Cave (Yuan et al., 2004, D4 in Fig. 4G). Climate conditions during MIS 3, which were similar to today or even warmer and wetter, are also reported from several other palaeoclimate proxy studies from the Asian monsoon domain including the Chinese Loess and Tibetan plateau, south-western China, and the South China Sea (see Herzschuh, 2006 and references therein). The results of palaeobotanical and isotope studies in northern and eastern Siberia led to the reconstruction of a more continental regional climate during the last glacial interval, including MIS 3 interstadial characterised by relatively high summer temperatures and/or a longer snow-free period and extremely low winter temperatures and precipitation (see Müller et al., 2010 for details and references). A visual comparison of the fossil and modern surface pollen spectra from Lake Billyakh (Müller et al., 2010) in the northern part of eastern Siberia and from Lake Kotokel (Bezrukova et al., 2010) in the southern part of eastern Siberia primarily points towards drier than present climate. Anderson and Lozhkin (2001) came to the conclusion that the western Beringian climate conditions were similar to today's between 39 and 33 ^{14}C ka BP (ca 43.2–37.5 cal. ka BP). As indicated by Overpeck et al. (1996) and Hodell et al. (1999) for the southern Asian monsoon domain, such favourable climate conditions as inferred from the Khoe pollen record and the above mentioned studies probably reflect the interplay between solar forcing and other glacial climate boundary conditions during MIS 3. While the summer insolation exceeded the present-day conditions (Laskar et al., 2004, Fig. 4J), its positive effect on the Asian summer monsoon intensity was suppressed by the NH continental ice sheets, low North Atlantic sea surface temperature (SST) and large-scale Asian snow cover. This is supported by Nakagawa et al. (2008), who postulated that during periods of minimum eccentricity (e.g. MIS 3) the control of solar forcing over the monsoon decreased relative to glacial forcing (i.e. the extent of global ice sheets).

As indicated by weighted averages of the MTCO and PANN values and larger error bars, the MIS 3 interstadial conditions are interrupted by a phase of distinctive climate deterioration around 39 cal. ka BP. A synchronous trend towards less favourable conditions is seen in decreasing values for tree cover (Fig. 4E) and in increasing NAP taxa percentages at this time interval (Fig. 2; Igarashi and Zharov, 2011), which appears to be coincident (within accuracy of the age model) with Heinrich event 4 (H4). H4 is described as the largest of the six North Atlantic cold events during the last glacial period (Hemming, 2004). As denoted by the MTCO and MTWA reconstructions, the temperature decline is attributed to the winter season, which might be related to widespread winter sea-ice across the North Atlantic Ocean (Denton et al., 2005). Significant shifts towards drier conditions during Heinrich events are also suggested for the Indian monsoon domain by elemental and grain size records from the Indus submarine slope in the northern Arabian Sea (Deplazes et al., 2014) and for the East Asian monsoon domain by stalagmite $\delta^{18}O$ records from the Hulu (Wang et al., 2001, Fig. 4G) and Sanbao (Wang et al., 2008) caves in China. Moreover, there is correspondence between the annual temperature reconstructions (T. Nakagawa, personal communication 2013) based on the SG06 high-resolution pollen record from Lake Suigetsu in central Japan (Nakagawa et al., 2012) and our results during H4. Although smaller in magnitude, the recognised phase of cooler conditions in central Japan is similarly pronounced in relation to MIS 3 climate fluctuations and nearly identical in timing. Given the robust chronology of the annually laminated sediment record SG06 (Bronk Ramsey et al., 2012), these correlations would in turn enhance the confidence for the age–depth model of the Khoe sedimentary succession. The more sensitive climate reaction denoted in our MAT results may be due to the location of the Khoe site at the northern limit of the EASM, which would lead to a stronger influence of cold Siberian air masses during phases of weak EASM circulation. Comparable relations between the position of palaeoclimate archives (ranging from central to outer monsoon zone) and the magnitude of precipitation variations over the Holocene interval are also identified for the ISM domain (Fleitmann et al., 2007; Leipe et al., 2014). We associate the decrease in average MTCO and PANN in combination with rather low min MTCO and PANN values at the end of MIS 3 (ca 29.7 cal. ka BP) with Heinrich event 3 (H3). In contrast to H4, the climate deterioration of H3 appears less pronounced. This might be a result of the lower temporal resolution in this part of the core section and/or shorter duration of a regional H3-related climate change. It also may indicate that the North Atlantic cooling had a much weaker impact on the climate of the study region than during H4.

5.3. The MIS 2 full glacial and Lateglacial interval (ca 29–11.7 cal. ka BP)

Within the full glacial section of the Khoe record (ca 29–16 cal. ka BP), which largely represents MIS 2, most samples are characterised by MAT-inferred reconstructions showing noticeably lower min values (Fig. 4A–D), thus suggesting generally cooler and drier annual conditions in the study region. After phase of climate fluctuations (ca 29–21.8 cal. ka BP), including several short pulses towards climate amelioration, annual temperature and precipitation decrease. Most unfavourable growing conditions are suggested during ca 21.8–15.3 cal. ka BP when lowest annual temperature and precipitation levels are parallelled by increased seasonality (Fig. 4A–D). Basically inorganic sediment and minimal sedimentation rates (Fig. 2) are likely a response to lowered biomass production due to climate deterioration during the last glacial interval.

The cold (MTCO = −30.5 °C) and dry (PANN = 470 mm) pulse around 20 cal. ka BP, which coincides with the simulated absolute minimum global sea level (Peltier and Fairbanks, 2006, Fig. 4I) lagging the NH summer insolation minimum (Laskar et al., 2004, Fig. 4J) by ca 3 ka is likely related to the LGM. The reconstructed mean value for MTCO is in agreement with averaged PMIP simulation results for the LGM (Jiang and Lang, 2010), which suggest winter temperature for the Khoe region between ca −28.5 and −33.5 °C. The cold/dry pulse identified in our reconstructions is synchronous with reconstructed minimum mean effective moisture based on a set of 75 palaeoclimate records from monsoonal Central Asia (Herzschuh, 2006) and much drier and cooler than present conditions in eastern China (Wang et al., 2001, Fig. 4G) and northern Japan (Igarashi et al., 1993; Igarashi, 1996).

Heinrich event 2 (H2) and 1 (H1) are less distinct in our climate and tree cover reconstructions in comparison with H4. However, H1 is suggested to be the longest stadial of the last glacial interval (Denton et al., 2010). It also appears to be well reflected in the stalagmite $\delta^{18}O$ records from China (Wang et al., 2001; Yuan et al., 2004, Fig. 4G). Possibly, the climate signals in the fossil pollen assemblages of the Khoe record during both events are obscured by lowest sedimentation rates between ca 29–15.3 cal. ka BP and relatively low temporal resolution. The subsequent climate amelioration towards the Holocene with a stepwise increase of

MTCO and PANN between ca 15.3–12.8 cal. ka BP is interrupted by a climate reversal between ca 12.8–11.7 cal. ka BP. Both reconstructed events are well in agreement with key palaeoclimate records from the North Atlantic region (e.g. Svensson et al., 2008, Fig. 4F), thus correspond to the late-glacial Bølling–Allerød interstadial and the Younger Dryas stadial, respectively, which are widely recognised within the Asian monsoon domain including coastal China (e.g. Wang et al., 2001; Yuan et al., 2004, Fig. 4G; Stebich et al., 2009) and central Japan (Nakagawa et al., 2005, 2006). A North Atlantic region-like pattern of deglacial warmer/moister and cooler/drier climate conditions is also evident in different fossil pollen records from the Hokkaido Region of northern Japan (Igarashi et al., 1993; Igarashi, 1996, 2013). According to the reconstruction, MTWA weighted averages are lowest during the late-glacial ca 15.3–11.9 cal. ka BP. We presume that this late-glacial MTWA decrease is related to the continuous rise in global sea level in response to large-scale deglaciation (Waelbroeck et al., 2002, Fig. 4H; Peltier and Fairbanks, 2006, Fig. 4I), which marks the transition from continental glacial to maritime interglacial climate in the Khoe record. Furthermore, the melting of the sea- and mountain ice would have led to the discharge of large amounts of cold water into the adjacent seas (i.e. Okhotsk Sea and Sea of Japan) and contribute to lowered summer temperatures on Sakhalin during the Lateglacial–Holocene transition. Though, extensive glaciation in the Okhotsk Sea region (e.g. Grosswald and Hughes, 2002) is not indicated by recent studies (e.g. Brigham-Grette, 2001; Melles et al., 2012), most of the authors agree that sea ice cover could play an important role for the Okhotsk Sea and Sakhalin environments during the full glacial and the Lateglacial interval (e.g. Sakamoto et al., 2005; Yamazaki et al., 2013; Gorbarenko et al., 2014).

5.4. The Holocene (ca 11.7 cal. ka BP – present)

The early Holocene (ca 11.7–8.7 cal. ka BP) is characterised by considerably warmer and wetter conditions compared to the Lateglacial period, with winters slightly cooler than today but precipitation levels comparable to modern conditions. The marked climate amelioration is supported by narrower uncertainty ranges and higher upper and lower reconstruction limits in contrast to the last glacial period. Although summer insolation peaked, Holocene climate optimum conditions did not occur in the study region before ca 8.7 cal. ka BP, which, at first glance, seems to be in agreement with review studies arguing for a middle Holocene climate optimum in the northern (Zhao and Yu, 2012; Ran and Feng, 2013) or entire (Herzschuh, 2006; Wang et al., 2010) domain of the EASM. In contrast, asynchrony with the ISM domain, where Holocene climate optimum conditions are identified during the early Holocene (see Leipe et al., 2014 and references therein), has been questioned by the works of different authors (e.g. Rudaya et al., 2009; Zhang et al., 2011; Li et al., 2014) and thus remains controversial. Different palynological studies from Hokkaido provide further evidence for a Holocene climate optimum not having occurred before ca 8 cal. ka BP (Sakaguchi, 1992; Igarashi et al., 2002, Igarashi et al., 2011), when pollen of cold-tolerant *Larix* disappeared from the records and pollen of the temperate broad-leaved taxon *Quercus* started to strongly increase. Although climate gradually ameliorated during the early Holocene stage, boreal conifer forest taxa prevailed (Igarashi et al., 2002; Igarashi et al., 2011). Correspondingly, middle Holocene optimum climate conditions are also inferred from studies in the lower Amur River basin (Mokhova et al., 2009; Bazarova et al., 2011) and on the Kuril Islands (Razjigaeva et al., 2013).

Holocene optimum climate with slightly increased precipitation and improved thermal conditions is reconstructed for the period ca 8.7–5.2 cal. ka BP. This is well in line with a major spread of cool mixed and cool conifer forests in Hokkaido and in the southern part of Sakhalin which is reflected by maximum pollen percentages for *Ulmus*, *Quercus*, *Fraxinus*, *Juglans*, *Corylus* and *Acer* (e.g. see Igarashi et al., 2002; Igarashi, 2013 and references therein). Although remaining on high levels, summer insolation had started to decrease, which indicates a mainly regional rather than orbital forcing of the early to middle Holocene climate conditions in northern Sakhalin. An important factor for the regional climate was probably the influence of the surrounding seas and ocean currents. By this time, the Sea of Japan had transgressed further north towards the modern Tatar Strait with its shoreline located fairly close to the Khoe sampling site. After its initial inflow to the Sea of Japan at the onset of the Holocene (e.g. Oba et al., 1991, 1995), the TWC (Fig. 1B), is suggested to have reached a phase of highest intensity between ca 9/8–7 cal. ka BP (Oba et al., 1991, 1995; Itaki et al., 2004; Takada et al., 2006). The TWC intensity probably culminated at around 8 cal. ka BP when according to Sawada and Handa (1998) the subtropical heat transport to northern latitudes of the Pacific Ocean reached a maximum. Furthermore, evidence for cool early Holocene conditions is found in the north-western and southern Okhotsk Sea. Records of ice rafted debris and marine diatom assemblages and alkenones suggest that SSTs were low until ca 9–8 cal. ka BP due to persistent sea ice influence and reached a maximum in the late middle Holocene at ca 4–5 cal. ka BP (Ternois et al., 2000; Gorbarenko et al., 2014).

Interestingly, climate optimum conditions are parallelled by a slight reduction in weighted averages of total tree cover compared to the previous Holocene interval. A possible reason for this is that tree growth is not necessarily directly related to precipitation, but depends on the annual moisture availability often expressed with α (Priestley–Taylor coefficient) as the ratio of actual evapotranspiration over potential evapotranspiration (Prentice et al., 1992), which also accounts for thermal conditions (Prentice et al., 1992). Hence, tree growth may be constrained by temperature-induced high evapotranspiration (i.e. low α) even when precipitation is at high levels. Similar findings are reported in a study of a fossil pollen record from the EASM domain in north-eastern China, where the Holocene peak period of tree pollen percentages is not in phase with warmest and wettest conditions but with the peak in MAT-based α reconstructions (Guiot et al., 2008). On the contrary, it might be also considered that higher precipitation levels were parallelled by increased moisture availability, which led to a large-scale expansion of bogs at the expense of forests. This hypothesis is supported by the high percentages of typical bog taxa like *Sphagnum* and *M. gale* in the fossil pollen and spore assemblages of the Khoe record (Fig. 2), which would in turn explain less favourable conditions for tree growth. Whether bog growth at that time was restricted to a rather small area at and around the sampled site or affected wider areas of Sakhalin need more study. A substantial impact on the vegetation by deforestation may yet be ruled out as the early inhabitants of Sakhalin are reported to have been subsisting on hunting, fishing and gathering (Lutaenko et al., 2007; Kuzmin and Rakov, 2011) and were likely not numerous and rather dispersed.

The uppermost interval (ca 5.2–0 cal. ka BP) is initiated by a swing towards a drier and on average cooler environment that culminated ca 4.4 cal. ka BP with a coeval interruption in the overall dominance of cool mixed forest taxa by taiga taxa. Subsequently, MTCO and PANN remained on a level that was lower than during the middle Holocene. This is broadly in agreement with palaeoclimate proxy studies from the entire Asian monsoon domain (e.g. Herzschuh, 2006; Fleitmann et al., 2007; Rudaya et al., 2009; Wang et al., 2010; Ran and Feng, 2013; Li et al., 2014) and the summer insolation decline (Laskar et al., 2004, Fig. 4J). Between ca

5.2–0 cal. ka BP, NAP and shrubby taxa expand while AP taxa decrease, which, according to Igarashi et al. (2002), is due to unstable climate conditions expressed by the fluctuation in dominant pollen taxa percentages and changes in forest composition. Analogous late Holocene climate trends are inferred on the basis of palynological investigations from the wider study region including the lower Amur River basin (Mokhova et al., 2009; Bazarova et al., 2011) and the Kuril Islands (Razjigaeva et al., 2013). However, late Holocene climate deterioration is less obvious in the fossil pollen records from Hokkaido, as suggested by the migration history of *Fagus crenata* (Japanese beech) (see Igarashi, 2013 for review and references). A recent quantitative climate and vegetation reconstruction derived from a ca 5500-year-old pollen record from south-western Hokkaido (Leipe et al., 2013) suggests that between ca 3.6 cal. ka BP and today, climate there was even slightly wetter and warmer during winter than the previous interval, which is likely caused by strengthening of the TWC. It seems well conceivable that a re-intensified TWC had a stronger influence on the regional and local climate conditions during the late Holocene than the weakening summer insolation (Fig. 4J). However, the lack of additional well-dated marine records from the northern Sea of Japan and terrestrial proxy records from Sakhalin and/or northern Japan prevents us from conducting a more robust and detailed interpretation.

Several Holocene short-term pulses towards climate deterioration are imprinted in the Khoe reconstructions (Fig. 4A–D). The most prominent cold/dry relapses are found at around 10.3, 9.3, 8.2, 7.4, 6.0, 4.4, 2.9, 1.5 and 0.5–0.9 cal. ka BP, and thus match well with the Holocene cold events recorded in the North Atlantic marine sediment (Bond et al., 1997, 2001) and Greenland ice cores (Mayewski et al., 1997, 2004). Such cold events are also reconstructed for other regions within the Asian monsoon domain (Hong et al., 2003; Wang et al., 2005b; Leipe et al., 2014) and the Okhotsk Sea (Gorbarenko et al., 2014). The driving mechanisms for these NH cold climate oscillations, which show no clear cyclicity but a fairly complex spatiotemporal pattern, are still insufficiently understood (Wanner et al., 2008). In order to clarify whether the short-term cold spells registered in the Khoe fossil pollen record represent a direct teleconnection with one or several of the identified processes, further high-resolution palaeoclimate proxy records are required from the study region.

6. Conclusions

The results of the MAT-based reconstruction of temperature, precipitation and percentage tree cover of the Khoe record show distinct changes in climate and environmental conditions.

Weighted averages of MTCO and PANN during MIS 3 are lower than present but generally similar to the late Holocene averages, suggesting interstadial conditions. Further reduced MTCO and PANN values are reconstructed during the following full glacial interval representing MIS 2.

The anti-phase relationship between MTCO and MTWA during the last glacial interval might be related to changes in the degree of continentality due to variations in the global sea level and glaciation. However, the average MTWA reconstructions should not be overinterpreted since the uncertainty ranges are rather large and the influence of summer temperatures on the boreal forests (and pollen assemblages) of the late Pleistocene is less important, as shown by vegetation models.

The Lateglacial interval is marked by an increase in MTCO and PANN, which broadly coincides with the Bølling–Allerød interstadial followed by the Younger Dryas oscillation towards colder and drier climate. Synchronously, MTWA reconstructions suggest that summer temperatures were slightly decreased, which we relate to more maritime conditions in response to rising global sea levels.

The climate during the Holocene interval is warmer and wetter with highest levels of tree cover in the study region. Reconstructed maximum tree cover indicates that annual moisture availability (α) was highest during the early Holocene (prior to ca 8.7 cal. ka BP) when, despite peak summer insolation, a rise in annual temperatures was suppressed by the influence of low SSTs of the surrounding seas. Middle Holocene climate optimum conditions ca 8.7–5.2 cal. ka BP are likely caused by the effect of high-level solar output, which was amplified by the rising global sea level (i.e. more maritime conditions) and intensified flow of the TWC in the Sea of Japan.

Supplementary material associated with this article is provided in the Open Access information system PANGAEA (http://www.pangaea.de/).

Acknowledgements

The work of C. Leipe was supported by the German Research Foundation (DFG) grant RI 809/24. P. Tarasov acknowledges the DFG Heisenberg Program (grant TA 540/5) and would like to express sincere gratitude to Yurij, whose excellent driving skills allowed access to the wildest places of Sakhalin for collecting reference pollen samples, and to Mr. Chiharu Abe, director of Hakodate Jomon Culture Center, who provided invaluable help during reference sample collection on Hokkaido. This work is an environmental contribution to the Baikal-Hokkaido Archaeology Project (http://bhap.artsrn.ualberta.ca/). We express our sincere gratitude to Dr. Yaeko Igarashi for kindly providing us original counts of the Khoe pollen record and important articles published in Japan and for making a number of critical comments to the early draft of this manuscript. We also gratefully acknowledge the helpful suggestions of two anonymous reviews. Last but not least, we greatly acknowledge G. Shephard for English proof reading.

References

Alexandrova, A.N., 1982. Pleistotsen Sakhalina. Nauka, Moscow (in Russian).
Alley, R.B., 2000. The Younger Dryas cold interval as viewed from central Greenland. Quat. Sci. Rev. 19 (1–5), 213–226.
Alpat'ev, A.M., Arkhangel'skii, A.M., Podoplelov, N.Y., Stepanov, A.Y., 1976. Fizicheskaya Geografiya SSSR (Aziatskaya Chast'). Vysshaya Shkola, Moscow (in Russian).
Anderson, P.M., Lozhkin, A.V., 2001. The stage 3 interstadial complex (Karginskii/middle Wisconsinan interval) of Beringia: variations in paleoenvironments and implications for paleoclimatic interpretations. Quat. Sci. Rev. 20, 93–125.
Andreev, A.A., Grosse, G., Schirrmeister, L., Kuzmina, S.A., Novenko, E.Y., Bobrov, A.A., Tarasov, P.E., Ilyashuk, B.P., Kuznetsova, T.V., Krbetschek, M., Meyer, H., Kunitsky, V.V., 2004. Late Saalian and Eemian palaeoenvironmental history of the Bol'shoy Lyakhovsky Island (Laptev Sea region, Arctic Siberia). Boreas 33 (4), 319–348.
Bartlein, P., Harrison, S., Brewer, S., Connor, S., Davis, B., Gajewski, K., Guiot, J., Harrison-Prentice, T., Henderson, A., Peyron, O., Prentice, I., Scholze, M., Seppä, H., Shuman, B., Sugita, S., Thompson, R., Viau, A., Williams, J., Wu, H., 2011. Pollen-based continental climate reconstructions at 6 and 21 ka: a global synthesis. Clim. Dyn. 37 (3), 775–802.
Bazarova, V.B., Klimin, M.A., Mokhova, L.M., Orlova, L.A., 2008. New pollen records of Late Pleistocene and Holocene changes of environment and climate in the Lower Amur River basin, NE Eurasia. Quat. Int. 179, 9–19.
Bazarova, V.B., Mokhova, L.M., Klimin, M.A., Kopoteva, T.A., 2011. Vegetation development and correlation of Holocene events in the Amur River basin, NE Eurasia. Quat. Int. 237 (1–2), 83–92.
Bezrukova, E.V., Tarasov, P.E., Solovieva, N., Krivonogov, S.K., Riedel, F., 2010. Last glacial-interglacial vegetation and environmental dynamics in southern Siberia: chronology, forcing and feedbacks. Palaeogeogr. Palaeoclimatol. Palaeoecol. 296, 185–198.
Bigelow, N.H., Brubaker, L.B., Edwards, M.E., Harrison, S.P., Prentice, I.C., Anderson, P.M., Andreev, A.A., Bartlein, P.J., Christensen, T.R., Cramer, W., Kaplan, J.O., Lozhkin, A.V., Matveyeva, N.V., Murray, D.F., McGuire, A.D., Razzhivin, V.Y., Ritchie, J.C., Smith, B., Walker, D.A., Gajewski, K., Wolf, V., Holmqvist, B.H., Igarashi, Y., Kremenetskii, K., Paus, A., Pisaric, M.F.J., Volkova, V.S., 2003. Climate change and Arctic ecosystems: 1. Vegetation

changes north of 55°N between the last glacial maximum, mid-Holocene, and present. J. Geophys. Research-Atmospheres 108 (D19), 8170. http://dx.doi.org/10.1029/2002jd002558.
Bond, G., Showers, W., Cheseby, M., Lotti, R., Almasi, P., deMenocal, P., Priore, P., Cullen, H., Hajdas, I., Bonani, G., 1997. A pervasive millennial-scale cycle in North Atlantic Holocene and glacial climates. Science 278, 1257–1266.
Bond, G., Kromer, B., Beer, J., Muscheler, R., Evans, M.N., Showers, W., Hoffmann, S., Lotti-Bond, R., Hajdas, I., Bonani, G., 2001. Persistent solar influence on North Atlantic climate during the Holocene. Science 294, 2130–2136.
Boyd, J.D., 1995. Descriptive physical oceanography of the North Pacific, Sea of Japan (East Sea) and Sea of Okhotsk. Arct. Res. 9, 72–80.
Brigham-Grette, J., 2001. New perspectives on Beringian Quaternary paleogeography, stratigraphy, and glacial history. Quat. Sci. Rev. 20 (1–3), 15–24.
Bronk Ramsey, C., Staff, R.A., Bryant, C.L., Brock, F., Kitagawa, H., van der Plicht, J., Schlolaut, G., Marshall, M.H., Brauer, A., Lamb, H.F., Payne, R.L., Tarasov, P.E., Haraguchi, T., Gotanda, K., Yonenobu, H., Yokoyama, Y., Tada, R., Nakagawa, T., 2012. A Complete terrestrial radiocarbon record for 11.2 to 52.8 kyr B.P. Science 338, 370–374.
Bukhteeva, A.V., Reimers, N.F., 1967. Vegetation map. In: Atlas Sakhalinskoi Oblasti. GUGK, Moscow, pp. 106–107.
Dansgaard, W., Johnsen, S.J., Clausen, H.B., Dahl-Jensen, D., Gundestrup, N.S., Hammer, C.U., Hvidberg, C.S., Steffensen, J.P., Sveinbjornsdottir, A.E., Jouzel, J., Bond, G., 1993. Evidence for general instability of past climate from a 250-kyr ice-core record. Nature 364, 218–220.
Danzeglocke, U., Jöris, O., Weninger, B., 2013. CalPal-2007online (accessed 09.09.13.). http://www.calpal-online.de/.
DeFries, R.S., Hansen, M.C., Townshend, J.R.G., Janetos, A.C., Loveland, T.R., 2000a. 1 Kilometer Tree Cover Continuous Fields, 1.0. Department of Geography, University of Maryland, College Park, Maryland, pp. 1992–1993.
DeFries, R.S., Hansen, M.C., Townshend, J.R.G., Janetos, A.C., Loveland, T.R., 2000b. A new global 1-km dataset of percentage tree cover derived from remote sensing. Glob. Change Biol. 6 (2), 247–254.
Denton, G.H., Alley, R.B., Comer, G.C., Broecker, W.S., 2005. The role of seasonality in abrupt climate change. Quat. Sci. Rev. 24, 1159–1182.
Denton, G.H., Anderson, R.F., Toggweiler, J.R., Edwards, R.L., Schaefer, J.M., Putnam, A.E., 2010. The last glacial termination. Science 328, 1652–1656.
Deplazes, G., Lückge, A., Stuut, J.-B.W., Pätzold, J., Kuhlmann, H., Husson, D., Fant, M., Haug, G.H., 2014. Weakening and strengthening of the Indian monsoon during Heinrich events and Dansgaard-Oeschger oscillations. Paleoceanography 29 (2). http://dx.doi.org/10.1002/2013PA002509, 2013PA002509.
Ding, Y.H., Chan, C.L., 2005. The East Asian summer monsoon: an overview. Meteorol. Atmos. Phys. 89 (1–4), 117–142.
Domrös, M., Peng, G., 1988. The Climate of China. Springer, Berlin.
Dykoski, C.A., Edwards, R.L., Cheng, H., Yuan, D., Cai, Y., Zhang, M., Lin, Y., Qing, J., An, Z., Revenaugh, J., 2005. A high-resolution, absolute-dated Holocene and deglacial Asian monsoon record from Dongge Cave, China. Earth Planet. Sci. Lett. 233 (1–2), 71–86.
Edwards, M.E., Anderson, P.M., Brubaker, L.B., Ager, T.A., Andreev, A.A., Bigelow, N.H., Cwynar, L.C., Eisner, W.R., Harrison, S.P., Hu, F.S., Jolly, D., Lozhkin, A.V., MacDonald, G.M., Mock, C.J., Ritchie, J.C., Sher, A.V., Spear, R.W., Williams, J.W., Yu, G., 2000. Pollen-based biomes for Beringia 18,000, 6000 and 0 ^{14}C yr BP. J. Biogeogr. 27 (3), 521–554.
ESRI, 2012. ArcGIS Desktop: Release 10.1. Environmental Systems Research Institute, Redlands, CA.
Fleitmann, D., Burns, S.J., Mangini, A., Mudelsee, M., Kramers, J., Villa, I., Neff, U., Al-Subbary, A.A., Buettner, A., Hippler, D., Matter, A., 2007. Holocene ITCZ and Indian monsoon dynamics recorded in stalagmites from Oman and Yemen (Socotra). Quat. Sci. Rev. 26 (1–2), 170–188.
Geograficheski Atlas SSSR. 1990. Glavnoe upravlenie geodezii i kartografii, Moskow (in Russian).
Gorbarenko, S.A., Artemova, A.V., Goldberg, E.L., Vasilenko, Y.P., 2014. The response of the Okhotsk Sea environment to the orbital-millennium global climate changes during the Last Glacial Maximum, deglaciation and Holocene. Glob. Planet. Change 116, 76–90.
Grimm, E.C., 1993. TILIA 2.0 Version b.4 (Computer Software). Illinois State Museum, Research and Collections Center, Springfield.
Grimm, E.C., 2004. TGView. Illinois State Museum, Research and Collections Center, Springfield.
Grosswald, M.G., Hughes, T.J., 2002. The Russian component of an Arctic ice sheet during the last glacial maximum. Quat. Sci. Rev. 21 (1–3), 121–146.
Guiot, J., 1990. Methodology of the last climatic cycle reconstruction in France from pollen data. Palaeogeogr. Palaeoclimatol. Palaeoecol. 80 (1), 49–69.
Guiot, J., Hai, H.B., Jiang, W.Y., Luo, Y.L., 2008. East Asian Monsoon and paleoclimatic data analysis: a vegetation point of view. Clim. Past 4, 137–145.
Heinrich, H., 1988. Origin and consequences of cyclic ice rafting in the Northeast Atlantic Ocean during the past 130,000 years. Quat. Res. 29 (2), 142–152.
Helmens, K.F., 2014. The Last Interglacial–Glacial cycle (MIS 5–2) re-examined based on long proxy records from central and northern Europe. Quat. Sci. Rev. 86, 115–143.
Hemming, S.R., 2004. Heinrich events: massive Late Pleistocene detritus layers of the North Atlantic and their global climate imprint. Rev. Geophys. 42 (1), RG1005. http://dx.doi.org/10.1029/2003RG000128.
Herzschuh, U., 2006. Palaeo-moisture evolution in monsoonal Central Asia during the last 50,000 years. Quat. Sci. Rev. 25 (1–2), 163–178.
Hodell, D.A., Brenner, M., Kanfoush, S.L., Curtis, J.H., Stoner, J.S., Xueliang, S., Yuan, W., Whitmore, T.J., 1999. Paleoclimate of southwestern China for the past 50,000 yr inferred from lake sediment records. Quat. Res. 52 (3), 369–380.
Hong, Y.T., Hong, B., Lin, Q.H., Zhu, Y.X., Shibata, Y., Hirota, M., Uchida, M., Leng, X.T., Jiang, H.B., Xu, H., Wang, H., Yi, L., 2003. Correlation between Indian Ocean summer monsoon and North Atlantic climate during the Holocene. Earth Planet. Sci. Lett. 211 (3–4), 371–380.
Hu, C., Henderson, G.M., Huang, J., Xie, S., Sun, Y., Johnson, K.R., 2008. Quantification of Holocene Asian monsoon rainfall from spatially separated cave records. Earth Planet. Sci. Lett. 266 (3–4), 221–232.
Igarashi, Y., 1996. A lateglacial climatic reversion in Hokkaido, northeast Asia, inferred from the *Larix* pollen record. Quat. Sci. Rev. 15 (10), 989–995.
Igarashi, Y., 2013. Holocene vegetation and climate on Hokkaido Island, northern Japan. Quat. Int. 290–291, 139–150.
Igarashi, Y., Zharov, A.E., 2011. Climate and vegetation change during the late Pleistocene and early Holocene in Sakhalin and Hokkaido, northeast Asia. Quat. Int. 237, 24–31.
Igarashi, Y., Igarashi, T., Daimaru, H., Yamada, O., Miyagi, T., Matsushita, K., Hiramatsu, K., 1993. Vegetation history of Kenbuchi Basin and Furano Basin in Hokkaido, North Japan, since 32,000 yrs BP. Quat. Res. 32, 89–105 (in Japanese with English abstract).
Igarashi, Y., Sagayama, T., Higake, T., Fukuda, M., 2000. Late Quaternary environmental change in central and north Sakhalin, Russia. J. Geogr. 109 (2), 165–173 (in Japanese with English abstract).
Igarashi, Y., Murayama, M., Igarashi, T., Higake, T., Fukuda, M., 2002. History of *Larix* forest in Hokkaido and Sakhalin, northeast Asia since the last glacial. Acta Palaeontol. Sin. 41 (4), 524–533.
Igarashi, Y., Yamamoto, M., Ikehara, K., 2011. Climate and vegetation in Hokkaido, northern Japan, since the LGM: pollen records from core GH02-1030 off Tokachi in the northwestern Pacific. J. Asian Earth Sci. 40 (6), 1102–1110.
Itaki, T., Ikehara, K., Motoyama, I., Hasegawa, S., 2004. Abrupt ventilation changes in the Japan Sea over the last 30 ky: evidence from deep-dwelling radiolarians. Palaeogeogr. Palaeoclimatol. Palaeoecol. 208 (3–4), 263–278.
Ivanov, A., 2002. The Far East. In: Shahgedanova, M. (Ed.), The Physical Geography of Northern Eurasia. Oxford University Press, Oxford, pp. 422–447.
Jackson, S.T., Williams, J.W., 2004. Modern analogs in Quaternary paleoecology: here today, gone yesterday, gone tomorrow? Annu. Rev. Earth Planet. Sci. 32, 495–537.
Jiang, D., Lang, X., 2010. Last Glacial Maximum East Asian Monsoon: results of PMIP simulations. J. Clim. 23 (18), 5030–5038.
Jin, L., Schneider, B., Park, W., Latif, M., Khon, V., Zhang, X., 2014. The spatial–temporal patterns of Asian summer monsoon precipitation in response to Holocene insolation change: a model-data synthesis. Quat. Sci. Rev. 85 (0), 47–62.
Ju, L., Wang, H., Jiang, D., 2007. Simulation of the Last Glacial Maximum climate over East Asia with a regional climate model nested in a general circulation model. Palaeogeogr. Palaeoclimatol. Palaeoecol. 248 (3–4), 376–390.
Juggins, S., 2007. C2 Version 1.5 User Guide. Software for Ecological and Palaeoecological Data Analysis and Visualisation. Newcastle University, Newcastle upon Tyne, UK.
Kageyama, M., Peyron, O., Pinot, S., Tarasov, P., Guiot, J., Joussaume, S., Ramstein, G., PMIP participating groups, 2001. The Last Glacial Maximum climate over Europe and western Siberia: a PMIP comparison between models and data. Clim. Dyn. 17 (1), 23–43.
Kienast, F., Schirrmeister, L., Siegert, C., Tarasov, P.E., 2005. Palaeobotanical evidence for warm summers in the East Siberian Arctic during the last cold stage. Quat. Res. 63 (3), 283–300.
Krestov, P., 2003. Forest vegetation of easternmost Russia (Russian Far East). In: Kolbek, J., Šrůtek, M., Box, E.O. (Eds.), Forest Vegetation of Northeast Asia. Springer, pp. 93–180.
Kuzmin, Y.V., Rakov, V.A., 2011. Environment and prehistoric humans in the Russian Far East and neighbouring East Asia: main patterns of interaction. Quat. Int. 237 (1–2), 103–108.
Laskar, J., Robutel, P., Joutel, F., Gastineau, M., Correia, A.C.M., Levrard, B., 2004. A long-term numerical solution for the insolation quantities of the Earth. Astron. Astrophys. 428 (1), 261–285.
Leipe, C., Demske, D., Tarasov, P.E., 2014. A Holocene pollen record from the northwestern Himalayan lake Tso Moriri: implications for palaeoclimatic and archaeological research. Quat. Int. 348, 93–112.
Leipe, C., Kito, N., Sakaguchi, Y., Tarasov, P.E., 2013. Vegetation and climate history of northern Japan inferred from the 5500-year pollen record from the Oshima Peninsula, SW Hokkaido. Quat. Int. 290–291, 151–163.
Li, Y., Wang, N.a., Zhou, X., Zhang, C., Wang, Y., 2014. Synchronous or asynchronous Holocene Indian and East Asian summer monsoon evolution: a synthesis on Holocene Asian summer monsoon simulations, records and modern monsoon indices. Glob. Planet. Change 116, 30–40.
Lisiecki, L.E., Raymo, M.E., 2005. A Pliocene–Pleistocene stack of 57 globally distributed benthic δ^{18}O records. Paleoceanography 20 (1), PA1003. http://dx.doi.org/10.1029/2004PA001071.
Lutaenko, K.A., Zhushchikhovskaya, I.S., Mikishin, Y.A., Popov, A.N., 2007. Mid-holocene climatic changes and cultural dynamics in the basin of the sea of japan and adjacent areas. In: Anderson, D.G., Maasch, K.A., Sandweis, D.H. (Eds.), Climate Change and Cultural Dynamics: a Global Perspective on Mid-Holocene Transitions. Elsevier, Amsterdam, pp. 331–406.

Martyn, D., 1992. Developments in Atmospheric Science 18 – Climates of the World. Elsevier, Amsterdam.
Masson-Delmotte, V., Schulz, M., Abe-Ouchi, A., Beer, J., Ganopolski, A., González Rouco, J.F., Jansen, E., Lambeck, K., Luterbacher, J., Naish, T., Osborn, T., Otto-Bliesner, B., Quinn, T., Ramesh, R., Rojas, M., Shao, X., Timmermann, A., 2013. Information from Paleoclimate archives. In: Stocker, T.F., Qin, D., Plattner, G.-K., Tignor, M., Allen, S.K., Boschung, J., Nauels, A., Xia, Y., Bex, V., Midgley, P.M. (Eds.), Climate Change 2013: the Physical Science Basis. Contribution of Working Group I to the Fifth Assessment Report of the Intergovernmental Panel on Climate Change. Cambridge University Press, Cambridge, United Kingdom and New York, NY, USA, pp. 383–464.
Mayewski, P.A., Meeker, L.D., Twickler, M.S., Whitlow, S., Yang, Q., Lyons, W.B., Prentice, M., 1997. Major features and forcing of high-latitude northern hemisphere atmospheric circulation using a 110,000-year-long glaciochemical series. J. Geophys. Res. Oceans 102 (C12), 26345–26366.
Mayewski, P.A., Rohling, E.E., Curt Stager, J., Karlén, W., Maasch, K.A., David Meeker, L., Meyerson, E.A., Gasse, F., van Kreveld, S., Holmgren, K., Lee-Thorp, J., Rosqvist, G., Rack, F., Staubwasser, M., Schneider, R.R., Steig, E.J., 2004. Holocene climate variability. Quat. Res. 62 (3), 243–255.
Melles, M., Brigham-Grette, J., Minyuk, P.S., Nowaczyk, N.R., Wennrich, V., DeConto, R.M., Anderson, P.M., Andreev, A.A., Coletti, A., Cook, T.L., Haltia-Hovi, E., Kukkonen, M., Lozhkin, A.V., Rosén, P., Tarasov, P., Vogel, H., Wagner, B., 2012. 2.8 Million years of Arctic climate change from Lake El'gygytgyn, NE Russia. Science 337, 315–320.
Mokhova, L., Tarasov, P., Bazarova, V., Klimin, M., 2009. Quantitative biome reconstruction using modern and late Quaternary pollen data from the southern part of the Russian Far East. Quat. Sci. Rev. 28 (25–26), 2913–2926.
Morrill, C., Overpeck, J.T., Cole, J.E., 2003. A synthesis of abrupt changes in the Asian summer monsoon since the last deglaciation. Holocene 13 (4), 465–476.
Müller, S., Tarasov, P.E., Andreev, A.A., Tütken, T., Gartz, S., Diekmann, B., 2010. Late Quaternary vegetation and environments in the Verkhoyansk Mountains region (NE Asia) reconstructed from a 50-kyr fossil pollen record from Lake Billyakh. Quat. Sci. Rev. 29 (17–18), 2071–2086.
Müller, S., Tarasov, P.E., Hoelzmann, P., Bezrukova, E.V., Kossler, A., Krivonogov, S.K., 2014. Stable vegetation and environmental conditions during the Last Glacial Maximum: new results from Lake Kotokel (Lake Baikal region, southern Siberia, Russia). Quat. Int. 348, 14–24.
Nakagawa, T., Tarasov, P.E., Nishida, K., Gotanda, K., Yasuda, Y., 2002. Quantitative pollen-based climate reconstruction in central Japan: application to surface and Late Quaternary spectra. Quat. Sci. Rev. 21 (18–19), 2099–2113.
Nakagawa, T., Kitagawa, H., Yasuda, Y., Tarasov, P.E., Gotanda, K., Sawai, Y., 2005. Pollen/event stratigraphy of the varved sediment of Lake Suigetsu, central Japan from 15,701 to 10,217 SG vyr BP (Suigetsu varve years before present): description, interpretation, and correlation with other regions. Quat. Sci. Rev. 24 (14–15), 1691–1701.
Nakagawa, T., Tarasov, P.E., Kitagawa, H., Yasuda, Y., Gotanda, K., 2006. Seasonally specific responses of the East Asian monsoon to deglacial climate changes. Geology 34 (7), 521–524.
Nakagawa, T., Okuda, M., Yonenobu, H., Miyoshi, N., Fujiki, T., Gotanda, K., Tarasov, P.E., Morita, Y., Takemura, K., Horie, S., 2008. Regulation of the monsoon climate by two different orbital rhythms and forcing mechanisms. Geology 36 (6), 491–494.
Nakagawa, T., Gotanda, K., Haraguchi, T., Danhara, T., Yonenobu, H., Brauer, A., Yokoyama, Y., Tada, R., Takemura, K., Staff, R.A., Payne, R., Bronk Ramsey, C., Bryant, C., Brock, F., Schlolaut, G., Marshall, M., Tarasov, P., Lamb, H., Suigetsu 2006 Project Members, 2012. SG06, a fully continuous and varved sediment core from Lake Suigetsu, Japan: stratigraphy and potential for improving the radiocarbon calibration model and understanding of late Quaternary climate changes. Quat. Sci. Rev. 36, 164–176.
Nakamura, Y., Krestov, P.V., 2005. Coniferous forests of the temperate zone of Asia. In: Andersson, F.A. (Ed.), Ecosystems of the World vol. 6: Coniferous Forests-sElsevier, Amsterdam, pp. 163–220.
New, M., Lister, D., Hulme, M., Makin, I., 2002. A high-resolution data set of surface climate over global land areas. Clim. Res. 21 (1), 1–25.
Oba, T., Kato, M., Kitazato, H., Koizumi, I., Omura, A., Sakai, T., Takayama, T., 1991. Paleoenvironmental changes in the Japan Sea during the last 85,000 years. Paleoceanography 6, 499–518. http://dx.doi.org/10.1029/91PA00560.
Oba, T., Murayama, M., Matsumoto, E., Nakamura, T., 1995. AMS-^{14}C ages of Japan Sea cores from the Oki Ridge. Quat. Res. 34, 289–296 (in Japanese with English abstract).
Overpeck, J.T., Webb, T., Prentice, I.C., 1985. Quantitative interpretation of fossil pollen spectra: dissimilarity coefficients and the method of modern analogs. Quat. Res. 23 (1), 87–108.
Overpeck, J., Anderson, D., Trumbore, S., Prell, W., 1996. The southwest Indian Monsoon over the last 18 000 years. Clim. Dyn. 12 (3), 213–225.
Peltier, W.R., Fairbanks, R.G., 2006. Global glacial ice volume and Last Glacial Maximum duration from an extended Barbados sea level record. Quat. Sci. Rev. 25 (23–24), 3322–3337.
Porter, S.C., An, Z., 1995. Correlation between climate events in the North Atlantic and China during the last glaciation. Nature 375 (6529), 305–308.
Prentice, I.C., Cramer, W., Harrison, S.P., Leemans, R., Monserud, R.A., Solomon, A.M., 1992. A global biome model based on plant physiology and dominance, soil properties and climate. J. Biogeogr. 19 (2), 117–134.
Prentice, I.C., Guiot, J., Huntley, B., Jolly, D., Cheddadi, R., 1996. Reconstructing biomes from palaeoecological data: a general method and its application to European pollen data at 0 and 6 ka. Clim. Dyn. 12 (3), 185–194.
Ran, M., Feng, Z., 2013. Holocene moisture variations across China and driving mechanisms: a synthesis of climatic records. Quat. Int. 313–314, 179–193.
Razjigaeva, N.G., Ganzey, L.A., Grebennikova, T.A., Belyanina, N.I., Mokhova, L.M., Arslanov, K.A., Chernov, S.B., 2013. Holocene climatic changes and vegetation development in the Kuril Islands. Quat. Int. 290–291, 126–138.
Rudaya, N., Tarasov, P., Dorofeyuk, N., Solovieva, N., Kalugin, I., Andreev, A., Daryin, A., Diekmann, B., Riedel, F., Tserendash, N., Wagner, M., 2009. Holocene environments and climate in the Mongolian Altai reconstructed from the Hoton-Nur pollen and diatom records: a step towards better understanding climate dynamics in Central Asia. Quat. Sci. Rev. 28 (5–6), 540–554.
Sakaguchi, Y., 1992. Cooling of Hokkaido around 9000 BP caused by permafrost meltwater burst. Bull. Department Geogr. Univ. Tokyo 24, 1–6.
Sakamoto, T., Ikehara, M., Aoki, K., Iijima, K., Kimura, N., Nakatsuka, T., Wakatsuchi, M., 2005. Ice-rafted debris (IRD)-based sea-ice expansion events during the past 100 kyrs in the Okhotsk Sea. Deep Sea Res. Part II: Top. Stud. Oceanogr. 52 (16–18), 2275–2301.
Sawada, K., Handa, N., 1998. Variability of the path of the Kuroshio ocean current over the past 25,000 years. Nature 392, 592–595.
Sokolov, S.J., Svjazeva, O.A., Ogureeva, G.N., 1977. Arealy Derev'ev I Kustarnikov SSSR 1. Nauka, Leningrad (in Russian).
Stebich, M., Mingram, J., Han, J., Liu, J., 2009. Late Pleistocene spread of (cool-) temperate forests in Northeast China and climate changes synchronous with the North Atlantic region. Glob. Planet. Change 65, 56–70.
Svensson, A., Andersen, K.K., Bigler, M., Clausen, H.B., Dahl-Jensen, D., Davies, S.M., Johnsen, S.J., Muscheler, R., Parrenin, F., Rasmussen, S.O., Röthlisberger, R., Seierstad, I., Steffensen, J.P., Vinther, B.M., 2008. A 60 000 year Greenland stratigraphic ice core chronology. Clim. Past 4, 47–57.
Takada, H., Itaki, T., Ikehara, K., Yamada, K., Takayasu, K., 2006. Significant Tsushima Warm Current during the Early–Middle Holocene along the San-in district coast inferred from foraminiferal profiles. Quat. Res. 45, 249–256 (in Japanese with English abstract).
Takahara, H., Igarashi, Y., Hayashi, R., Kumon, F., Liew, P.-M., Yamamoto, M., Kawai, S., Oba, T., Irino, T., 2010. Millennial-scale variability in vegetation records from the East Asian Islands: Taiwan, Japan and Sakhalin. Quat. Sci. Rev. 29 (21–22), 2900–2917.
Tarasov, P.E., Webb III, T., Andreev, A.A., Afanas'eva, N.B., Berezina, N.A., Bezusko, L.G., Blyakharchuk, T.A., Bolikhovskaya, N.S., Cheddadi, R., Chernavskaya, M.M., Chernova, G.M., Dorofeyuk, N.I., Dirksen, V.G., Elina, G.A., Filimonova, L.V., Glebov, F.Z., Guiot, J., Gunova, V.S., Harrison, S.P., Jolly, D., Khomutova, V.I., Kvavadze, E.V., Osipova, I.M., Panova, N.K., Prentice, I.C., Saarse, L., Sevastyanov, D.V., Volkova, V.S., Zernitskaya, V.P., 1998. Present-day and mid-Holocene biomes reconstructed from pollen and plant macrofossil data from the former Soviet Union and Mongolia. J. Biogeogr. 25 (6), 1029–1053.
Tarasov, P.E., Peyron, O., Guiot, J., Brewer, S., Volkova, V.S., Bezusko, L.G., Dorofeyuk, N.I., Kvavadze, E.V., Osipova, I.M., Panova, N.K., 1999. Last Glacial Maximum climate of the former Soviet Union and Mongolia reconstructed from pollen and plant macrofossil data. Clim. Dyn. 15 (3), 227–240.
Tarasov, P.E., Volkova, V.S., Webb III, T., Guiot, J., Andreev, A.A., Bezusko, L.G., Bezusko, T.V., Bykova, G.V., Dorofeyuk, N.I., Kvavadze, E.V., Osipova, I.M., Panova, N.K., Sevastyanov, D.V., 2000. Last glacial maximum biomes reconstructed from pollen and plant macrofossil data from Northern Eurasia. J. Biogeogr. 27 (3), 609–620.
Tarasov, P., Granoszewski, W., Bezrukova, E., Brewer, S., Nita, M., Abzaeva, A., Oberhansli, H., 2005. Quantitative reconstruction of the last interglacial vegetation and climate based on the pollen record from Lake Baikal, Russia. Clim. Dyn. 25 (6), 625–637.
Tarasov, P.E., Williams, J.W., Andreev, A., Nakagawa, T., Bezrukova, E., Herzschuh, U., Igarashi, Y., Müller, S., Werner, K., Zheng, Z., 2007. Satellite- and pollen-based quantitative woody cover reconstructions for northern Asia: verification and application to Late-Quaternary pollen data. Earth Planet. Sci. Lett. 264 (1–2), 284–298.
Tarasov, P.E., Nakagawa, T., Demske, D., Österle, H., Igarashi, Y., Kitagawa, J., Mokhova, L., Bazarova, V., Okuda, M., Gotanda, K., Miyoshi, N., Fujiki, T., Takemura, K., Yonenobu, H., Fleck, A., 2011. Progress in the reconstruction of Quaternary climate dynamics in the Northwest Pacific: a new modern analogue reference dataset and its application to the 430-kyr pollen record from Lake Biwa. Earth Sci. Rev. 108 (1–2), 64–79.
Ternois, Y., Kawamura, K., Ohkouchi, N., Keigwin, L., 2000. Alkenone sea surface temperature in the Okhotsk Sea for the last 15 kyr. Geochem. J. 34, 283–293.
Waelbroeck, C., Labeyrie, L., Michel, E., Duplessy, J.C., McManus, J.F., Lambeck, K., Balbon, E., Labracherie, M., 2002. Sea-level and deep water temperature changes derived from benthic foraminifera isotopic records. Quat. Sci. Rev. 21 (1–3), 295–305.
Wang, B., 2006. The Asian Monsoon. Praxis Publishing Ltd, Chichester, 787 pp.
Wang, Y.J., Cheng, H., Edwards, R.L., An, Z.S., Wu, J.Y., Shen, C.C., Dorale, J.A., 2001. A high-resolution absolute-dated Late Pleistocene monsoon record from Hulu Cave, China. Science 294, 2345–2348.
Wang, P., Clemens, S., Beaufort, L., Braconnot, P., Ganssen, G., Jian, Z., Kershaw, P., Sarnthein, M., 2005a. Evolution and variability of the Asian monsoon system: state of the art and outstanding issues. Quat. Sci. Rev. 24 (5–6), 595–629.
Wang, Y.J., Cheng, H., Edwards, R.L., He, Y., Kong, X., An, Z., Wu, J., Kelly, M.J., Dykoski, C.A., Li, X., 2005b. The Holocene Asian monsoon: links to solar changes and North Atlantic climate. Science 308, 854–857.

Wang, Y., Cheng, H., Edwards, R.L., Kong, X., Shao, X., Chen, S., Wu, J., Jiang, X., Wang, X., An, Z., 2008. Millennial- and orbital-scale changes in the East Asian monsoon over the past 224,000 years. Nature 451, 1090–1093.

Wang, Y., Liu, X., Herzschuh, U., 2010. Asynchronous evolution of the Indian and East Asian Summer Monsoon indicated by Holocene moisture patterns in monsoonal central Asia. Earth-Sci. Rev. 103 (3–4), 135–153.

Wanner, H., Beer, J., Bütikofer, J., Crowley, T.J., Cubasch, U., Flückiger, J., Goosse, H., Grosjean, M., Joos, F., Kaplan, J.O., Küttel, M., Müller, S.A., Prentice, I.C., Solomina, O., Stocker, T.F., Tarasov, P., Wagner, M., Widmann, M., 2008. Mid- to Late Holocene climate change: an overview. Quat. Sci. Rev. 27 (19–20), 1791–1828.

Weninger, B., Jöris, O., 2008. A ^{14}C age calibration curve for the last 60 ka: the Greenland-Hulu U/Th timescale and its impact on understanding the Middle to Upper Paleolithic transition in Western Eurasia. J. Hum. Evol. 55 (5), 772–781.

Weninger, B., Jöris, O., Danzeglocke, U., 2013. CalPal-2007. Cologne Radiocarbon Calibration & Palaeoclimate Research Package (accessed 06.05.13.). http://www.calpal.de/.

Williams, J.W., Jackson, S.T., 2003. Palynological and AVHRR observations of modern vegetational gradients in eastern North America. Holocene 13 (4), 485–497.

Williams, J.W., Tarasov, P., Brewer, S., Notaro, M., 2011. Late Quaternary variations in tree cover at the northern forest-tundra ecotone. J. Geophys. Res. Biogeosci. 116, G01017. http://dx.doi.org/10.1029/2010jg001458.

Wu, B., Wang, J., 2002. Winter Arctic oscillation, Siberian High and East Asian Winter Monsoon. Geophys. Res. Lett. 29 (19), 1897. http://dx.doi.org/10.1029/2002gl015373.

Yamazaki, T., Inoue, S., Shimono, T., Sakamoto, T., Saburo Sakai, S., 2013. Sea-ice conditions in the Okhotsk Sea during the last 550 kyr deduced from environmental magnetism. Geochem. Geophys. Geosyst. 14 (12), 5026–5040. http://dx.doi.org/10.1002/2013GC004959.

Yuan, D., Cheng, H., Edwards, R.L., Dykoski, C.A., Kelly, M.J., Zhang, M., Qing, J., Lin, Y., Wang, Y., Wu, J., Dorale, J.A., An, Z., Cai, Y., 2004. Timing, duration, and transitions of the Last Interglacial Asian Monsoon. Science 304, 575–578.

Zhang, J., Chen, F., Holmes, J.A., Li, H., Guo, X., Wang, J., Li, S., Lü, Y., Zhao, Y., Qiang, M., 2011. Holocene monsoon climate documented by oxygen and carbon isotopes from lake sediments and peat bogs in China: a review and synthesis. Quat. Sci. Rev. 30 (15–16), 1973–1987.

Zhao, J.-X., Wang, Y.-J., Collerson, K.D., Gagan, M.K., 2003. Speleothem U-series dating of semi-synchronous climate oscillations during the last deglaciation. Earth Planet. Sci. Lett. 216 (1–2), 155–161.

Zhao, Y., Yu, Z., 2012. Vegetation response to Holocene climate change in East Asian monsoon-margin region. Earth-Sci. Rev. 113 (1–2), 1–10.

Zheng, Y., Zheng, Z., Tarasov, P., Qian, L., Huang, K., Wei, J., Luo, C., Xu, Q., Lu, H., Luo, Y., 2010. Palynological and satellite-based MODIS observations of modern vegetational gradients in China. Quat. Int. 218, 190–201.

Zhulidov, A.V., Headley, J.V., Robarts, R.D., Nikanorov, A.M., Ischenko, A.A., 1997. Atlas of Russian Wetlands: Biogeography and Metal Concentrations. National Hydrology Research Institute, Saskatchewan, 309 pp.